NUREG/CR–4667, Vol. 13
ANL–92/6

Environmentally Assisted Cracking in Light Water Reactors

Semiannual Report
April–September 1991

Prepared by
T. F. Kassner, W. E. Ruther, H. M. Chung, P. D. Hicks,
A. G. Hins, J. Y. Park, W. K. Soppet, W. J. Shack

Argonne National Laboratory

Prepared for
U.S. Nuclear Regulatory Commission

AVAILABILITY NOTICE

Availability of Reference Materials Cited in NRC Publications

Most documents cited in NRC publications will be available from one of the following sources:

1. The NRC Public Document Room, 2120 L Street, NW., Lower Level, Washington, DC 20555

2. The Superintendent of Documents, U.S. Government Printing Office, P.O. Box 37082, Washington, DC 20013-7082

3. The National Technical Information Service, Springfield, VA 22161

Although the listing that follows represents the majority of documents cited in NRC publications, it is not intended to be exhaustive.

Referenced documents available for inspection and copying for a fee from the NRC Public Document Room include NRC correspondence and internal NRC memoranda; NRC bulletins, circulars, information notices, inspection and investigation notices; licensee event reports; vendor reports and correspondence; Commission papers; and applicant and licensee documents and correspondence.

The following documents in the NUREG series are available for purchase from the GPO Sales Program: formal NRC staff and contractor reports, NRC-sponsored conference proceedings, international agreement reports, grant publications, and NRC booklets and brochures. Also available are regulatory guides, NRC regulations in the *Code of Federal Regulations*, and *Nuclear Regulatory Commission Issuances*.

Documents available from the National Technical Information Service include NUREG-series reports and technical reports prepared by other Federal agencies and reports prepared by the Atomic Energy Commission, forerunner agency to the Nuclear Regulatory Commission.

Documents available from public and special technical libraries include all open literature items, such as books, journal articles, and transactions. *Federal Register* notices, Federal and State legislation, and congressional reports can usually be obtained from these libraries.

Documents such as theses, dissertations, foreign reports and translations, and non-NRC conference proceedings are available for purchase from the organization sponsoring the publication cited.

Single copies of NRC draft reports are available free, to the extent of supply, upon written request to the Office of Administration, Distribution and Mail Services Section, U.S. Nuclear Regulatory Commission, Washington, DC 20555.

Copies of industry codes and standards used in a substantive manner in the NRC regulatory process are maintained at the NRC Library, 7920 Norfolk Avenue, Bethesda, Maryland, for use by the public. Codes and standards are usually copyrighted and may be purchased from the originating organization or, if they are American National Standards, from the American National Standards Institute, 1430 Broadway, New York, NY 10018.

NUREG/CR--4667-Vol.13

TI92 009721

Environmentally Assisted Cracking in Light Water Reactors

Semiannual Report
April–September 1991

Manuscript Completed: January 1992
Date Published: March 1992

Prepared by
T. F. Kassner, W. E. Ruther, H. M. Chung, P. D. Hicks,
A. G. Hins, J. Y. Park, W. K. Soppet, W. J. Shack

Argonne National Laboratory
9700 South Cass Avenue
Argonne, IL 60439

Prepared for
Division of Engineering
Office of Nuclear Regulatory Research
U.S. Nuclear Regulatory Commission
Washington, DC 20555
NRC FINs A2212, A2256

Previous Documents in Series

Environmentally Assisted Cracking in Light Water Reactors Annual Report October 1983—September 1984, NUREG/CR-4287, ANL-85-33 (June 1985).

Light-Water-Reactor Safety Materials Engineering Research Programs: Quarterly Progress Report October—December 1984, NUREG/CR-3998 Vol. III, ANL-84-60 Vol. III (October 1985).

Light-Water-Reactor Safety Materials Engineering Research Programs: Quarterly Progress Report January—March 1985, NUREG/CR-4490 Vol. I, ANL-85-75 Vol. I (March 1986).

Environmentally Assisted Cracking in Light Water Reactors Semiannual Report April—September 1985, NUREG/CR-4667 Vol. I, ANL-86-31 (June 1986).

Environmentally Assisted Cracking in Light Water Reactors Semiannual Report October 1985—March 1986, NUREG/CR-4667 Vol. II, ANL-86-37 (September 1987).

Environmentally Assisted Cracking in Light Water Reactors Semiannual Report April—September 1986, NUREG/CR-4667 Vol. III, ANL-87-37 (September 1987).

Environmentally Assisted Cracking in Light Water Reactors Semiannual Report October 1986—March 1987, NUREG/CR-4667 Vol. IV, ANL-87-41 (December 1987).

Environmentally Assisted Cracking in Light Water Reactors Semiannual Report April—September 1987, NUREG/CR-4667 Vol. V, ANL-88-32 (June 1988).

Environmentally Assisted Cracking in Light Water Reactors Semiannual Report October 1987—March 1988, NUREG/CR-4667 Vol. 6, ANL-89/10 (August 1989).

Environmentally Assisted Cracking in Light Water Reactors Semiannual Report April—September 1988, NUREG/CR-4667 Vol. 7, ANL-89/40 (March 1990).

Environmentally Assisted Cracking in Light Water Reactors Semiannual Report October 1988—March 1989, NUREG/CR-4667 Vol. 8, ANL-90/4 (June 1990).

Environmentally Assisted Cracking in Light Water Reactors Semiannual Report April—September 1989, NUREG/CR-4667 Vol. 9, ANL-90/48 (March 1991).

Environmentally Assisted Cracking in Light Water Reactors Semiannual Report October 1989—March 1990, NUREG/CR-4667 Vol. 10, ANL-91/5 (March 1991).

Environmentally Assisted Cracking in Light Water Reactors Semiannual Report April—September 1990, NUREG/CR-4667 Vol. 11, ANL-91/9 (May 1991).

Environmentally Assisted Cracking in Light Water Reactors Semiannual Report October 1990—March 1991, NUREG/CR-4667 Vol. 12, ANL-91/24 (August 1991).

Environmentally Assisted Cracking in Light Water Reactors

by

T. F. Kassner, W. E. Ruther, H. M. Chung, P. D. Hicks,
A. G. Hins, J. Y. Park, W. K. Soppet, and W. J. Shack

Abstract

This report summarizes work performed by Argonne National Laboratory on fatigue and environmentally assisted cracking in light water reactors during the six months from April 1991 to September 1991. Fatigue and environmentally assisted cracking of piping, pressure vessels, and core components in light water reactors are important concerns as extended reactor lifetimes are envisaged. Topics that have been investigated during this year include (1) fatigue and stress corrosion cracking (SCC) of low-alloy steel used in piping and in steam generator and reactor pressure vessels, (2) the roles of chromate and sulfate in simulated boiling water reactor (BWR) water on SCC of sensitized Type 304 SS, and (3) radiation-induced segregation (RIS) and irradiation-assisted SCC of Type 304 SS after accumulation of relatively high fluence. Fatigue data were obtained on medium-sulfur-content A533-Gr B and A106-Gr B pressure-vessel and piping steels in high-purity (HP) deoxygenated water, in simulated pressurized water reactor (PWR) water, and in air. Crack-growth-rate (CGR) measurements on composite specimens of A533-Gr B/Inconel-182/Inconel-600 (plated with nickel) and on homogeneous specimens of A533-Gr B material (plated with gold, nickel, or nickel-chromium) indicate that CGRs increased markedly during small-amplitude cyclic loading in HP water with ≈300 ppb dissolved oxygen. Under cyclic loading, crack growth was observed at maximum stress intensity values that produced no crack growth under constant (R = 1) loading. The CGR dependence on dissolved-oxygen concentration (0.3 to 30 ppm) was also investigated under different loading conditions. Possible synergistic reactions involving chromate and sulfate in SCC of sensitized Type 304 SS have been investigated by fracture-mechanics CGR tests. Low chromate concentrations in BWR water (25-35 ppb) may actually have a beneficial effect on SCC if the sulfate concentration is below a critical level. Failures of reactor-core internal components in BWRs and PWRs after accumulation of relatively high fluence have been attributed to RIS of Si, P, S, Ni, and Cr; however, the degree to which RIS produces susceptibility to irradiation-assisted SCC is unclear. Microchemical and microstructural changes in HP and commercial-purity (CP) Type 304 SS specimens from control-blade absorber tubes used in two operating BWRs were studied by Auger electron spectroscopy and scanning electron microscopy, and slow-strain-rate-tensile tests were conducted on tubular specimens in air and in simulated BWR water at 289°C. Susceptibility of the CP absorber tubes to intergranular stress corrosion cracking (IGSCC) was similar to that of other CP heats of Types 304 and 316 SS reported in the literature. However, the HP absorber tubes exhibited greater IGSCC susceptibility than did the CP materials. High SCC susceptibility seems to be consistent with irradiation-induced Cr depletion at grain boundaries, which was more significant in the HP heat than in the CP heat.

Contents

Figures

Tables

Executive Summary

Fatigue of Ferritic Piping and Pressure Vessel Steels

Plain carbon steels are used extensively in PWR and BWR nuclear steam supply systems as piping and pressure vessel materials. The steels of interest for these applications include A106–Gr B and A333–Gr 6 for seamless pipe and A302–Gr B, A508–2, and A533–Gr B plate for pressure vessels. Additional fatigue tests were conducted on medium–sulfur–content A106–Gr B piping and A533–Gr B pressure vessel steels in simulated PWR water and in air. The fatigue life of A533–Gr B steel in deoxygenated water is generally shorter by a factor of 2 than that in air. No significant effect of the aqueous environments was observed in tests on A106–Gr B steel. The effects of load shape and loading rate will be further explored in subsequent testing.

Stress Corrosion Cracking of Ferritic Steels

The crack growth rate (CGR) curves in Section XI of the ASME Boiler and Pressure Vessel Code are based on load ratios $R \leq 0.9$. Our recent work at $R = 0.95$ indicates that the threshold stress intensity factor (and magnitude) of the CGRs predicted by the current Section XI correlations are nonconservative at very high load ratios. Based on the hypothesis that environmental enhancement of the CGR is a function of crack tip strain rate, equations that relate CGRs to loading parameters have been modified to incorporate high–R data. Additional fracture–mechanics CGR tests have been performed on a composite specimen of A533–Gr B/Inconel–182/Inconel–600 plated with nickel, and on homogeneous specimens of A106–Gr B and A533–Gr B (plated with nickel–chromium) material. The effects of load history and dissolved–oxygen content on the CGRs of the composite specimen were examined. The CGRs increased markedly during small–amplitude cyclic loading ($R = 0.95$). Under the cyclic loading, crack growth was observed at maximum stress intensity values that produced no crack growth under constant $R = 1$ loading. Under $R = 0.95$ loading, relatively high CGRs (2×10^{-9} m·s^{-1}) were observed in HP water containing ≈300 ppb dissolved oxygen. When the specimen is in the low–CGR regime (2×10^{-11} m·s^{-1}), increasing the dissolved–oxygen concentration to 6 ppm or higher initiated a return to the high CGR regime, at least at an R value of 0.95.

Effects of Chromate and Sulfate on SCC of Type 304 SS

Current BWR operating practices have reduced to very low levels the ingress of ionic impurities (e.g., sulfate, chloride) into the coolant system. Soluble corrosion products, viz., chromate and the counterbalancing hydronium ion, are now the major ionic species present. Because only a small fraction of the recirculation water in BWRs passes through the reactor water cleanup system, the concentration of chromate ions in the reactor water can be much greater than in the feedwater (e.g., ≈25–35 ppb versus <1 ppb, respectively). Possible synergistic reactions involving chromate and sulfate in SCC of sensitized Type 304 SS were investigated by fracture–mechanics CGR tests. The results indicate that the CGRs of sensitized Type 304 SS under high–R, low–frequency loading are low ($<4 \times 10^{-11}$ m·s^{-1}), provided that the chromate/sulfate concentration ratio in oxygenated feedwater is >3. Thus, a low chromate concentration in BWR water (25–35 ppb) may

actually have a beneficial effect on SCC, provided that the sulfate concentration is below a critical level (i.e., ≈10 ppb).

Irradiation-Assisted Stress Corrosion Cracking of Type 304 SS

Failures of austenitic SS after accumulation of high fluence have been attributed to radiation-induced segregation (RIS) or depletion of elements such as Si, P, S, Ni, and Cr. However, the exact identity of the elements that segregate and the degree to which RIS produces susceptibility of the core-internal components of LWRs to irradiation assisted (IA) SCC are unclear. High- and commercial-purity (HP and CP, respectively) Type 304 SS specimens were obtained from control-blade absorber tubes used in two operating BWRs. SSRT tests were conducted on tubular specimens in air and in simulated BWR water at 289°C. Results in air showed that the yield and ultimate tensile strengths of the HP material were higher than those of the CP material for a comparable fluence. Stress versus elongation characteristics of the SSRT specimens were consistent with results of SEM analyses of the percent IGSCC on fracture surfaces. IGSCC susceptibility of the present CP absorber tubes was similar to those of other CP heats of Types 304 and 316 SS reported in the literature. However, the HP absorber tubes exhibited greater IGSCC susceptibility than did the CP materials. It is difficult to explain the relatively high susceptibility of the HP material on the basis of Si or P segregation, because impurity segregation in the HP absorber tubes was negligible for all fluence levels. Rather, the high susceptibility seems to be consistent with the observation that irradiation-induced Cr depletion was more significant in the HP heat than in the CP heat, indicating that irradiation-induced grain-boundary depletion of Cr is the primary process in IASCC, at least in simulated BWR water.

1 Introduction

Fatigue and environmentally assisted cracking of piping, pressure vessels, and core components in light water reactors (LWRs) are important concerns as extended reactor lifetimes are envisaged. The degradation processes include intergranular stress corrosion cracking (IGSCC) of austenitic stainless steel (SS) piping in boiling water reactors (BWRs), and propagation of fatigue or SCC cracks (which initiate in sensitized SS cladding) into low-alloy ferritic steels in BWR pressure vessels.* Similar cracking has also occurred in upper shell-to-transition cone girth welds in pressurized water reactor (PWR) steam generator vessels** and cracks have been found in steam generator feedwater distribution piping.*** Another concern is failure of reactor-core internal components after accumulation of relatively high fluence, which has occurred in both BWRs and PWRs. The general pattern of the observed failures indicates that, as nuclear plants age and the neutron fluence increases, a wide variety of apparently nonsensitized austenitic materials become susceptible to intergranular failure by a degradation process commonly known as irradiation-assisted stress-corrosion cracking (IASCC). Some of the failures have been reported for components that are subjected to relatively low or negligible stress levels, e.g., control-blade sheaths and handles and instrument dry tubes of BWRs. Although most failed components can be replaced, some safety-significant structural components, such as the BWR top guide, shroud, and core plate, would be very difficult or impractical to replace. Research during the past year focused on (1) fatigue and SCC of ferritic steels used in piping and in steam generator and reactor pressure vessels, (2) role of chromate and sulfate in simulated BWR water in SCC of sensitized Type 304 SS, and (3) IASCC in high- and commercial-purity Type 304 SS specimens from control-blade absorber tubes used in two operating BWRs.

2 Fatigue of Ferritic Steels

Section III of the ASME Boiler and Pressure Vessel Code recognizes fatigue as a possible mode of failure in pressure vessel steels and piping materials. For the case of many cycles, the primary concern is the endurance limit, which is the stress that can be applied an infinite number of times without producing failure. In pressure vessels, however, the number of stress cycles applied during the design life seldom exceeds 10^5 and is frequently only several thousand.[1] The main difference between high- and low-cycle fatigue (prevalent in pressure vessels) is that the former involves little plastic deformation. However, failure in a few thousand cycles can only be produced by strains well in excess of yield strain. In the plastic region, large changes in strain are produced by small changes in stress. Fatigue damage in the plastic region has been found to be a function of plastic strain, and fatigue curves for use in this region should be based on tests in which strain rather than stress is the controlled variable.

---

*USNRC Information Notice No. 90-29, "Cracking of Cladding in Its Heat Affected Zone in the Base Metal of a Reactor Vessel Head," April 30, 1990.

**USNRC Information Notice No. 90-04, "Cracking of the Upper Shell-to-Transition Cone Girth Welds in Steam Generators," January, 26, 1990.

***USNRC Information Notice No. 91-19, "Steam Generator Feedwater Distribution Piping Damage," March 12, 1991.

2.1 Technical Progress (P. D. Hicks and W. J. Shack)

Plain carbon and low-alloy steels are used extensively in PWR and BWR nuclear steam supply systems as piping and pressure-vessel materials. The steels of interest in these applications include A106-Gr B and A333-Gr 6 for seamless pipe and A302-Gr B, A508-2, and A533-Gr B plate for pressure vessels. The current Section III fatigue curves for carbon and low-alloy steels are based on tests in air at room temperature.[1] Tests in air at reactor operating temperatures show some deviation from the ASME mean data curve, but all data lie above the ASME design curve.[2] However, in tests at high strain amplitudes in oxygenated water, the fatigue lives of carbon steels are significantly decreased, and in some cases failures were observed below the ASME Section Design Curve.[3,4] Iida et al.[5] studied the fatigue of alloys equivalent to A508-Cl3 and A333-Cl6 in deionized water at temperatures up to 290°C. They showed that in oxygenated water at large strain amplitudes, fatigue lives were reduced in tests at lower strain rates. The magnitude of the decrease depended strongly on alloy composition, temperature, and concentration of dissolved oxygen in the water. At dissolved-oxygen concentrations of <100 ppb, the aqueous environment had little effect on the fatigue life of either alloy.

Nagata et al.[6] performed fatigue tests on forged ASTM A508 Cl-3 and on the rolled-equivalent ASTM A533-Gr B Cl-1 under strain control (at various strain rates) in pure water at several dissolved-oxygen levels. Water containing 100 ppb dissolved oxygen had very little effect on the fatigue behavior of both alloys at a strain rate of 1×10^{-3} s^{-1}, compared to the results of tests in air. Alloy A508 also showed little effect of strain rate, whereas a decrease in strain rate by up to two orders of magnitude decreased the fatigue life of A533-Gr B steel. Nagata et al.[6] attributed this to initiation effects due to the higher sulfide content of the A533-Gr B steel compared to the A508 material. They argue that A533-Gr B is more susceptible to surface pitting near manganese sulfide (MnS) inclusions, and the surface pitting near these inclusions decreases the initiation time for cracking. The lower strain rates simply provide more time for the pitting to occur. All tests were at a strain range of 0.7-0.8% and a strain rate of 0.1% with a triangular wave form. For dissolved-oxygen levels >1 ppm, the fatigue lives of both alloys decreased by up to 66%. However, it should be noted that Iida et al.[5] saw very little environmental effect in the high-cycle regime where initiation would be expected to dominate even in high-sulfur materials.

Terrell[7] tested A106-Gr B in PWR environments. For cyclic frequency in the range of 1.0-0.017 Hz, the fatigue life of smooth test specimens was virtually unaffected by the environment, whereas a small decrease in life occurred for notched specimens in tests at the lowest frequency. However, all data lie above the ASME design curve.

2.1.1 Experimental Methods

Additional uniaxial fatigue tests were conducted on A533-Gr B pressure vessel and A106-Gr B piping steels in water and in air. Initial results were presented in the previous report.[8] The A533-Gr B material for the test specimens was obtained from the lower head of the Midland Reactor, which was scrapped before the plant was completed. The medium-sulfur-content (0.016% S) steel had a tempered bainitic microstructure in the as-fabricated condition. Specimens of A106-Gr B containing 0.014% S were obtained from a piece of 20-in.-diameter schedule 140 pipe fabricated by the Cameron Iron Works,

Houston, TX. The chemical analyses of these two materials and of the ferritic and austenitic steels used in CGR tests are given in Table 1.

Fatigue tests were performed on smooth (1.0-μm surface-polished gage length, 19 mm) cylindrical hourglass-type specimens. During polishing of the specimen gage length, pullout of MnS inclusions occasionally occurred, tending to scuff the surface of the specimen. These inclusions were visible under a low-power microscope and appeared as slight surface roughness. The final polish of the specimen gage length was in a lengthwise direction to prevent circumferential scratches that might act as stress raisers during fatigue. The specimens were loaded uniaxially with a triangular wave form at a strain rate of 4×10^{-3} s^{-1}.

Tests were first performed in air at 288°C, under strain control at zero mean strain measured with an axial extensometer. Strain ranges of 1.0, 0.75, 0.50, and 0.35% were selected. The stroke response was recorded so that subsequent fatigue tests in water could be run in stroke control. This experimental procedure avoids difficulties associated with using a strain extensometer in a pressurized-water environment. After obtaining the strain

Table 1. Chemical Composition (wt.%) of Ferritic and Austenitic Steels in Fatigue[a,b] and Compact-Tension Specimens[b-g]

Material	C	P	S	Si	Fe	Cr	Ni	Mn	Mo	Ta/Nb	Ti
A533-Gr B[a]	0.20	0.014	0.016	0.17	Bal	0.19	0.50	1.28	0.47	–	–
A106-Gr B[b]	0.29	0.014	0.014	0.28	Bal	0.19	0.11	0.92	0.04	–	–
A533-Gr B[c]	0.23	0.005	0.004	0.27	Bal	0.12	0.70	1.42	0.56	–	–
A533-Gr B[d,e]	0.22	0.012	0.018	0.22	Bal	0.12	0.69	1.45	0.53	–	–
IN-182[f]	0.10	0.03	0.01	1.0	10.0	14.0	65.0	7.0	–	1.75	1.0
IN-600	0.07	–	0.001	0.19	9.41	15.23	73.84	0.30	–	0.12	0.31
Type 304 SS[g]	0.06	0.019	0.007	0.48	Bal	18.70	8.00	1.63	0.20	–	–

[a]Medium-sulfur-content steel for fatigue specimens was obtained from the lower head of the Midland Reactor. Material was used to fabricate fatigue specimens.

[b]Heat No. J-7201 (20-in.-diameter schedule 140 pipe) fabricated by the Cameron Iron Works, Houston, TX. Material was used to fabricate fatigue and crack-growth-rate specimens.

[c]Heat No A5401 for crack-growth-rate tests on 1T specimens in simulated BWR water.

[d]Composite Alloy-600/In-182/A533-Gr B compact tension (1T) specimen was fabricated such that the low-alloy steel was in the T-L orientation according to the ASTM nomenclature. Other 1TCT specimens of low-alloy steel were also in the T-L orientation.

[e]A533-Gr B Class 1 plate (Heat No. A-1195-1) was obtained from the Oak Ridge National Laboratory HSST Program. Material was used to fabricate fatigue specimens.

[f]Nominal composition of undiluted Inconel-182 weld metal (AWS Type ENiCrFe-3 per AWS Specification A5.11). A layer, ≈6 mm thick, was buttered to the A533-Gr B plate with a 3/32-in.-diameter weld rod and the material was heat treated at 621°C for 24 h and air-cooled. Inconel-600 (Heat No. NX5922-G11) was electron-beam-welded to the Inconel-182 to form the 1TCT specimen. Entire specimen was nickel-plated.

[g]Heat No. 30956 for crack-growth-rate tests on 1T specimens in simulated BWR water.

control data in air, a repeat test was performed under stroke control in air at 288°C. The mean stroke and stroke amplitude settings for these tests were the same as the stroke values obtained at the half-lives of the strain control tests. During the stroke-control tests, the strain was accurately monitored to give a better indication of the true strain experienced by the specimens when they are tested in water under stroke control. The strain amplitude in amplitude-versus-fatigue-life plots corresponds to that at the specimen half-life, as determined in high-temperature tests in air under stroke control.

Tests were conducted in high-purity (HP) deoxygenated water and in simulated PWR water at a flow rate of 8 $mL \cdot min^{-1}$ in a small autoclave (annular volume of 12 mL) at 288°C and a system pressure of 9 MPa. The nominal water chemistries are given in Table 2. Simulated PWR water was formulated by dissolving HP boric acid and lithium hydroxide in 20 L of deionized water before adding the solution to 132-L SS feedwater tanks. For tests in deionized water, the dissolved-oxygen concentration was reduced to <10 ppb by bubbling nitrogen through the water. A vacuum was drawn on the tank gas outlet to speed deoxygenation. After the dissolved oxygen was reduced to the desired level, a 20-kPa overpressure of nitrogen was maintained on the feedwater tank. Preparation of the simulated PWR water was similar, except that a 20-kPa overpressure of hydrogen was sustained to maintain ≈2 ppm dissolved hydrogen in the deoxygenated feedwater. Water from the once-through system was discarded in the drain.

Table 2. Nominal Water Chemistries for Fatigue Tests

Water Chemistry	Deionized Water	PWR Water
Conductivity ($\mu S \cdot cm^{-1}$)	0.17	25
pH (room temperature)	5.8	6.6
Dissolved O_2 (ppb)	<10	<10
Boron (ppm)	–	1000
Lithium (ppm)	–	2
Chloride (ppm)	<0.03	<0.03
Fluoride (ppm)	<0.01	<0.01
Dissolved H_2 (cm^3/kg)	–	18

2.1.2 Results

The fatigue test results on A533-Br B and A106-Gr B steels are summarized in Tables 3 and 4 and Figs. 1 and 2, respectively. The number of cycles to failure (N_{25} in Tables 3 and 4) is determined when the tensile stress amplitude decreases to 75% of the value observed at one-half the fatigue life. For the most part, the fatigue-life data are reasonably consistent. However, the fatigue lives of A533-Gr B specimens in Tests 1539 and 1542 in Table 3 varied by almost a factor of nine, although the loading and environmental conditions were the same in both tests. No factors such as a high concentration of manganese sulfide inclusions were found on the fracture surfaces to explain this variability in fatigue life. The fatigue lives of A533-Gr B steel in deoxygenated water are generally shorter than those in air (Fig. 1). However, Test 1533 at the lower strain rate of 4×10^{-5} s^{-1} showed no additional decrease in life, in contrast to the strong dependence of fatigue life on strain rate for high-sulfur steels in simulated BWR environments.[5]

Table 3. A533–Gr B Steel Test Conditions and Fatigue Lives

Test No.	Total Strain Range, $\Delta\varepsilon_t$ (Test Control)	Environment (at 288°C)	Cycles = N_{25}
1505	0.50% (strain)	Air	31,200
1508	1.00% (strain)	Air	3,305
1515	0.75% (strain)	Air	6,792
1517	0.35% (strain)	Air	2,053,295
1522	≈0.89% (stroke)	Air	3,419
1523	≈0.90% (stroke)	Air	2,200
1524	≈0.94% (stroke)	Air	3,714
1525	≈0.45% (stroke)	Air	65,758
1526	≈0.90% (stroke)	Deionized water	3,330
1527	≈0.45% (stroke)	Deionized water	10,334
1528	≈0.45% (stroke)	Deionized water	25,890
1529	≈0.45% (stroke)	PWR water	31,751
1530	≈0.90% (stroke)	PWR water	1,355
1533[a]	≈0.90% (stroke)	PWR water	3,416
1538	≈0.39% (stroke)	Air	>1,000,000
1539	≈0.39% (stroke)	PWR water	136,969
1542	≈0.39% (stroke)	PWR water	>1,154,892
1545	≈0.91% (stroke)	PWR water	3,264

[a]Positive sawtooth test: tensile-going strain rate of 4×10^{-5} s^{-1} (slower by 100X than the other tests) and a compression-going rate of 4×10^{-3} s^{-1}.

Fatigue data for both steels are plotted in Fig. 3 in terms of the pseudostress $S_a = E(\Delta\varepsilon_t/2)$, where $\Delta\varepsilon_t$ is the strain range, and E is Young's modulus (namely, 200 GPa for A533–Gr B steel). The data can be compared with curves in the ASME Boiler and Pressure Vessel Code (Section III) "Design Fatigue Curves for Carbon, Low Alloy and High Tensile Steels for Metal Temperatures not Exceeding 700°F."[1] The ASME Section III mean–data curve is also included in the figure.

Our fatigue data for A106–Gr B steel are consistent with data obtained by Terrell[7] in simulated PWR water (<10 ppb dissolved oxygen) where no noticeable effect of frequency or environment on fatigue life of this alloy was found (Fig. 3). The results are also consistent with the data of Prater and Coffin[9,10] and Iida et al.,[5] in which the effects of environment were minimal at dissolved oxygen levels of <100–200 ppb. All data at higher stress amplitudes tend to fall further below the the ASME mean–data curve than do data at longer lives.

Table 4. A106-Gr B Steel Test Conditions[a] and Fatigue Lives

Test No.	Total Strain Range, $\Delta\varepsilon_t$ (Test Control)	Environment (at 288°C)	Cycles = N_{25}
1498	1.00% (strain)	Air	1,051
1543	0.50% (strain)	Air	14,525
1546	≈1.03% (stroke)	Air	1,365
1547	≈1.03% (stroke)	PWR water	692
1548	0.50 % (stroke)	Air	10,632
1549	0.50% (stroke)	PWR water	9,396
1552	0.35 % (strain)	Air	93,322
1553	0.75% (strain)	Air	3,253

[a]Positive sawtooth tests with a tensile-going strain rate of 4×10^{-3} s^{-1}.

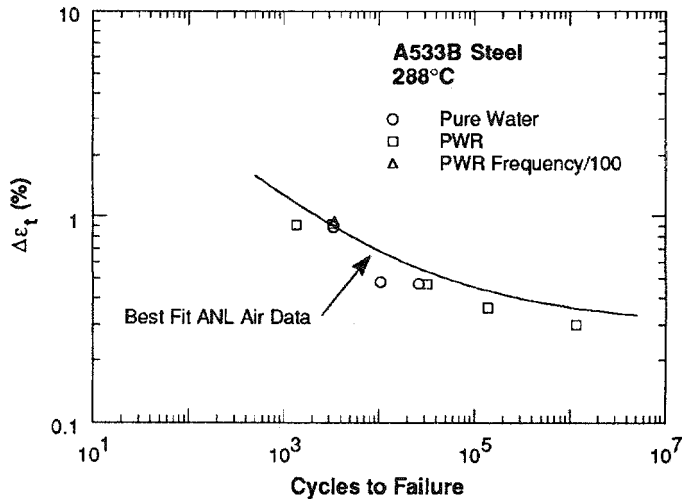

Figure 1. Total strain range vs. fatigue-life data for A533-Gr B Cl 1 steel at 288°C

3 Environmentally Assisted Cracking of Ferritic Steels

Over the past 15 years, the corrosion fatigue properties of low-alloy steels in LWR primary-system water chemistries have been studied extensively.[11-14] Much less information is available on SCC of these materials.[15-19] Because it is clear that very high crack-growth rates (CGRs) can occur in some materials under some combinations of loading and environment, the objective of the current work is to better define the circumstances that can produce SCC in these steels.

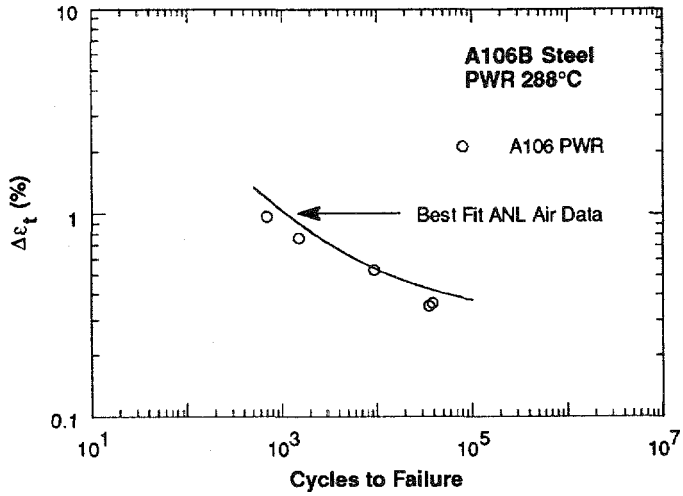

Figure 2. Total strain range vs. fatigue-life data for A106-Gr B steel at 288°C

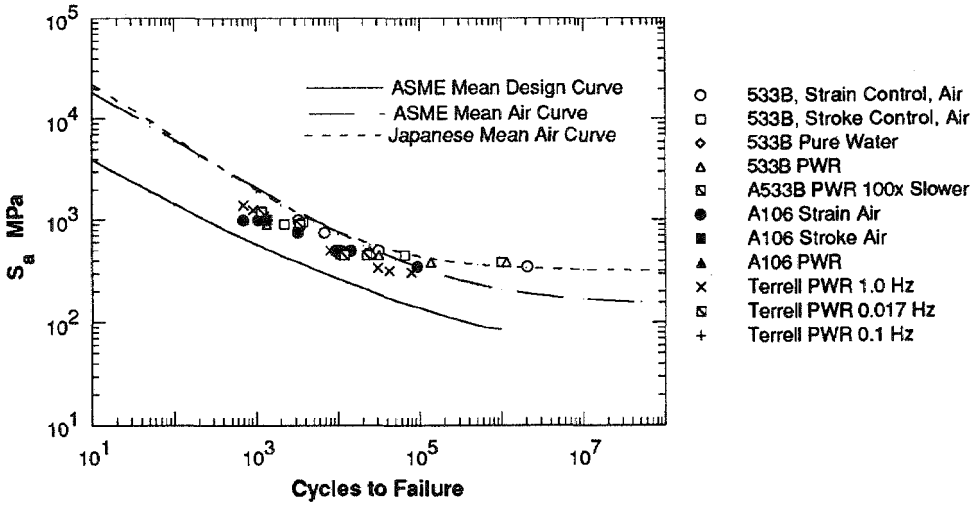

Figure 3. Elastic pseudostress vs. fatigue-life data for A533-Gr B Cl 1 and A106-Gr B steels at 288°C

3.1 Technical Progress

Fracture-mechanics CGR tests have been carried out on compact-tension specimens from low- and medium-sulfur-content heats (0.004 and 0.018 wt.%) of A533-Gr B pressure vessel steel, a medium-sulfur-content (0.014%) A106-Gr B piping steel, and a composite specimen of A533-Gr B/Inconel-182/Inconel-600 plated with nickel (chemical compositions are given in Table 1). One of the A533-Gr B specimens was nickel-chromium

plated to better simulate a clad ferritic steel vessel, where only the low-alloy steel at the crack surface is exposed to the environment. Surface films on the nickel-chromium and on nickel- and gold-plated specimens tested previously[20] are different from those on the nonplated ferritic specimens. Because virtually all of the existing data have been obtained on specimens without cladding, it is important to verify that those results were not unduly affected by the character of the surface film.

3.1.1 Crack-Growth-Rate Tests on Composite Inconel-182/A533-Gr-B Specimens (W. E. Ruther, T. F. Kassner, and W. K. Soppet)

The composite A533-Gr B/Inconel-182/Inconel-600 specimen (plated with nickel) was tested in simulated BWR water with ≈200 ppb dissolved oxygen at 289°C under cyclic loading with a positive sawtooth wave form (12-s loading and 1-s unloading times) at 0.08 Hz, load ratios ($R = K_{min}/K_{max}$) of 0.9 to 1.0, and maximum stress intensities, K_{max}, of ≈28 to 62 MPa·m$^{1/2}$. Crack-length measurements in conventional and plated specimens were made by a DC-potential-drop technique. Because no potential-drop calibration was available for the composite specimen, crack length was measured by the compliance method.

3.1.2 Results

Results from SCC tests on the composite specimen are given in Table 5. The fatigue precrack in the specimen traversed the Inconel-182 weld metal so that the initial 7.2 mm of crack growth over a time interval of 1000 h (Test 1) occurred in the underlying A533-Gr B material at an average rate of 2.0×10^{-9} m·s^{-1}. The K_{max} increased from 28 to 35 MPa·m$^{1/2}$. No periods of crack arrest or transient crack growth occurred during this phase of the test. This CGR is virtually identical to the "average" value for a previous composite specimen (2.3×10^{-9} m·s^{-1}), which included several crack extensions of 1-2 mm within ≈170-h time intervals, followed by ≈800-h periods of very slow steady-state growth.[21] For no apparent reason, the CGR of the composite specimen in the current test decreased abruptly at ≈1050 h to a very low value that continued over a period of ≈1000 h. This behavior is similar to that observed in the previous experiment.[21]

In Test 2, the K_{max} of the composite specimen was increased to 40 MPa·m$^{1/2}$ at an R of 0.95. Although an increase of K_{max} in the previous experiment[21] generally resulted in a brief increase in CGR, no such increase was noted during the next 300-h period in this test. After that period, the dissolved-oxygen concentration in the feedwater was increased to ≈30 ppm (Test 3). This action initiated a return to the high-CGR regime, which we allowed to persist for two weeks. The feedwater was then returned to the normal dissolved-oxygen concentration of ≈0.4 ppm in Test 4, and shortly thereafter the CGR returned to a low level (7.6×10^{-11} m·s^{-1}) for 800 h. The dissolved-oxygen level was then increased to 6 ppm in Test 5, and two days later rapid crack growth resumed. These experiments indicate that dissolved-oxygen concentration is an important variable at a load ratio of 0.95.

Table 5. Crack Growth of Inconel-182/A533-Gr B Composite Specimen[a] at Constant Load and Low-Frequency, High-R Loading[b] in High-Purity Water Containing ≈0.3 to 30 ppm Dissolved Oxygen at 289°C

		Water Chemistry			Electrode Potential		CGR Parameters			
Test No.	Time, h	Cond., μS·cm^{-1}	pH at 25°C	Oxygen,[c] ppm	304 SS, mV(SHE)	Pt, mV(SHE)	Load Ratio	K_{max},[d] MPa·m$^{1/2}$	ΔK,[e] MPa·m$^{1/2}$	Growth Rate, m·s^{-1}
1	0–1058	0.16	6.25	0.3	112	126	0.95	35.0	1.75	2.0 x 10^{-9}
	1058–2156							37.0	1.85	3.0 x 10^{-11}
2	2156–2492	0.13	6.20	0.3	49	82	0.95	40.0	2.00	3.0 x 10^{-11}
3	2492–2827	0.15	6.24	30	260	323	0.95	49.1	2.46	3.1 x 10^{-9}
4	2827–3666	0.12	6.27	0.4	96	137	0.95	50.5	2.53	7.6 x 10^{-11}
5	3666–3834	0.15	6.19	5.9	198	231	0.95	58.6	2.93	6.9 x 10^{-9}
6	3834–5005	0.13	6.36	6	183	204	1.0	59.0	0	2.5 x 10^{-11}
7	5009–6069	0.17	6.27	30	220	222	1.0	60.0	0	8.1 x 10^{-11}
8	6069–6379	0.14	6.33	31	205	204	0.98	60.1	1.20	3.8 x 10^{-11}
9	6379–6573	0.14	6.34	28	223	219	0.95	60.2	3.01	3.8 x 10^{-11}
10	6573–6592	0.14	6.34	28	220	215	0.90	62.4	6.24	7.8 x 10^{-9}

[a]Composite compact tension specimen (1TCT) (No. 02C-11) was fabricated from Inconel-600/Inconel-182/A533-Gr B Steel (Heat No. A-1195-1). Specimen was electroplated with nickel.

[b]Frequency of the positive sawtooth wave form was 8 x 10^{-2} Hz; rise time of 12 s and fall time of 1 s.

[c]Effluent dissolved-oxygen concentrations below 20 ppm were determined with an Orbisphere dissolved-oxygen meter; higher values were measured with CHEMetrics™ ampules.

[d]Maximum stress intensity, K_{max}, value at the end of each time period.

[e]$\Delta K = K_{max}(1 - R)$, where the load ratio $R = K_{min}/K_{max}$.

In the next series of tests, the effect of load ratio was investigated. In Test 6, the load ratio was increased from 0.95 to 1.0 (i.e., constant load); shortly thereafter, the CGR returned to the low level even though the dissolved-oxygen level remained at 6 ppm. The low CGR persisted for an additional 1200 h, after which the dissolved-oxygen level was increased to ≈30 ppm in Test 7. This caused a modest increase in CGR over an additional exposure period of 800 h. The load ratio was then decreased to 0.98 in Test 8 and the CGR decreased slightly during an additional 310-h period. The load ratio was decreased further to 0.95 in Test 9 and the CGR remained at the same low value (3.8 x 10^{-11} m·s^{-1}) over a 200-h interval. In Test 10, the load ratio was decreased to 0.9, and within 24 h, crack growth resumed a high rate (7.8 x 10^{-9} m·s^{-1}). The test was terminated after ≈20 h because the crack length exceeded the maximum allowable value. Even at a high K level (62 MPa·m$^{1/2}$), a load ratio of <1 is required to initiate a high CGR. No crack growth occurred in a conventional (nonplated) A533-Gr B specimen at a stress

intensity factor of 28.7 MPa·m$^{1/2}$ over the entire ≈6600-h experiment under the different environmental and loading conditions.

At the end of the test, the specimens were sectioned for metallographic examination. An SEM photograph of the fracture surface of the composite specimen (No. O2C-11), the crack path near the crack-tip region, and the fracture surface of half the specimen at low magnification are shown in Fig. 4(A). Photomicrographs of the entire fatigue precrack and the crack-tip region of the conventional companion specimen (No. O2C-12) are shown in Fig. 4(B). The fatigue crack in the latter specimen is filled with corrosion product.

The CGR results in Table 5 at different dissolved-oxygen levels and load ratios fall into two ranges, i.e., ≈2 to 8 x 10^{-11} and ≈2 to 8 x 10^{-9} m·s^{-1}. High CGRs occurred at an R of 0.95 in water containing 0.3, 6, and 30 ppm dissolved oxygen (Tests 1, 5, and 3, respectively). Low CGRs were also measured at this R value in water containing ≈0.3-0.4 and 28 ppm dissolved oxygen (Tests 2, 4, and 9). As mentioned previously, under constant load (R = 1.0), an increase in dissolved-oxygen concentration from 6 to 30 ppm produced a relatively small increase in the CGRs (Tests 6 and 7). A significant decrease in load ratio from 1.0 to 0.9 (sequentially in Tests 7-10) caused an abrupt transition to the high-CGR regime at an R of 0.9 in water containing ≈30 ppm dissolved oxygen.

These results, along with those from a previous composite specimen in which unusually large jumps in crack length (≈1-2 mm) occurred whenever K_{max} was increased (followed by periods of relatively slow crack growth),[21] indicate that triggering events in the environment and/or in the loading conditions can produce abrupt changes in the CGRs by two orders of magnitude. For example, increases in dissolved-oxygen concentration and K_{max} and decreases in load ratio can lead to high CGRs. Conversely, a transition from the high- to low-CGR regime can occur by decreasing the dissolved-oxygen concentration or by increasing the load ratio. However, steady-state CGRs can lie in either the high- or low-CGR regime for any given set of loading or environmental conditions. This is illustrated in Fig. 5, which summarizes the results in Table 5 at an R of 0.95 for composite specimen 02C-11, the composite specimen (02C-1) from a previous experiment,[21] and data from gold-plated and nonplated specimens of the same heat of ferritic steel.[20,21]

The heavy lines in Fig. 5 represent the predicted dependence of CGR on K_{max} for ferritic steels in 289°C water at an R of 0.95 and a rise-time T_R of 10 s, according to the fatigue CGR curves for ferritic steels in LWR environments proposed recently by Eason.* The model predicts a threshold for a transition from a low, nonenvironmentally assisted CGR to a much higher rate. The threshold K_{max} predicted by the model (which includes high-oxygen environments that may be more aggressive than those used in tests on which the model is based) is somewhat higher than the present data would indicate. The persistence of low CGRs above the "threshold" is consistent with a hysteresis observed in similar tests at lower R values in other investigations. One can "move up" the lower curve above the threshold without triggering high CGRs, but once high rates are achieved they persist at lower K_{max} levels. The interpretation of the present tests in terms of the

*Personal Communication, David Jones, Chairman MPC Task Force on Crack Propagation Technology, to W. J. Shack, Argonne National Laboratory, August 1991.

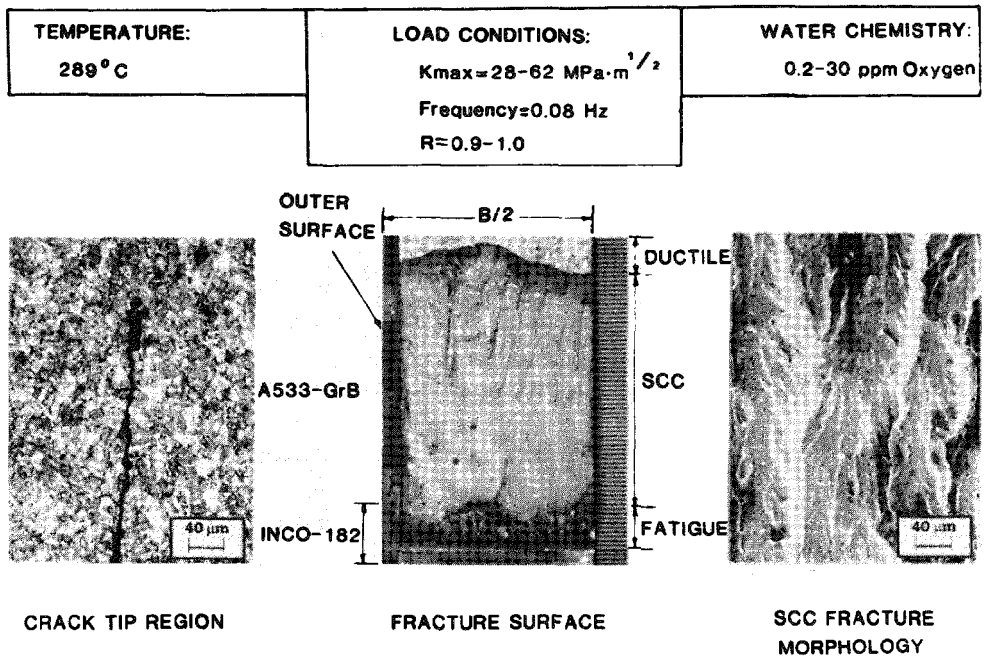

(A)

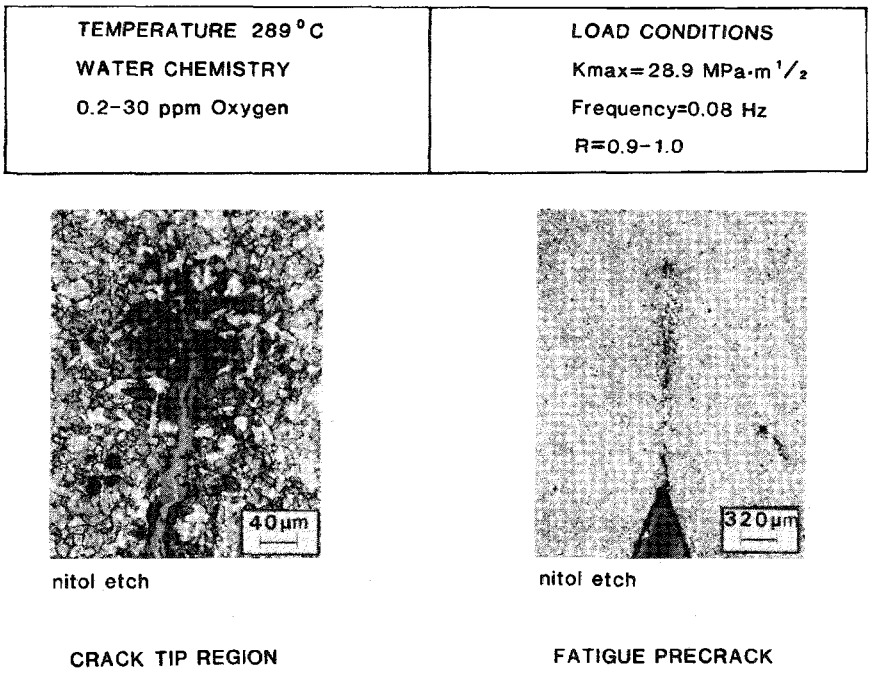

(B)

Figure 4. (A) crack path, fracture surface, and SCC fracture morphology of an 1TCT composite Inconel-182/A533-Gr B specimen (no. 02C-11) and (B) fatigue precrack of a conventional A533-Gr B specimen (no. 02C-12) after a crack growth experiment in high-purity oxygenated water at 289°C

threshold model is complicated because we have not run "classical" threshold tests with a fixed environment and a fixed R. The threshold is a function of R and probably of oxygen level. Instead of the single illustrative curve shown in Fig. 5, there should be a family of curves corresponding to the different conditions. The single curve is representative but not necessarily predictive.

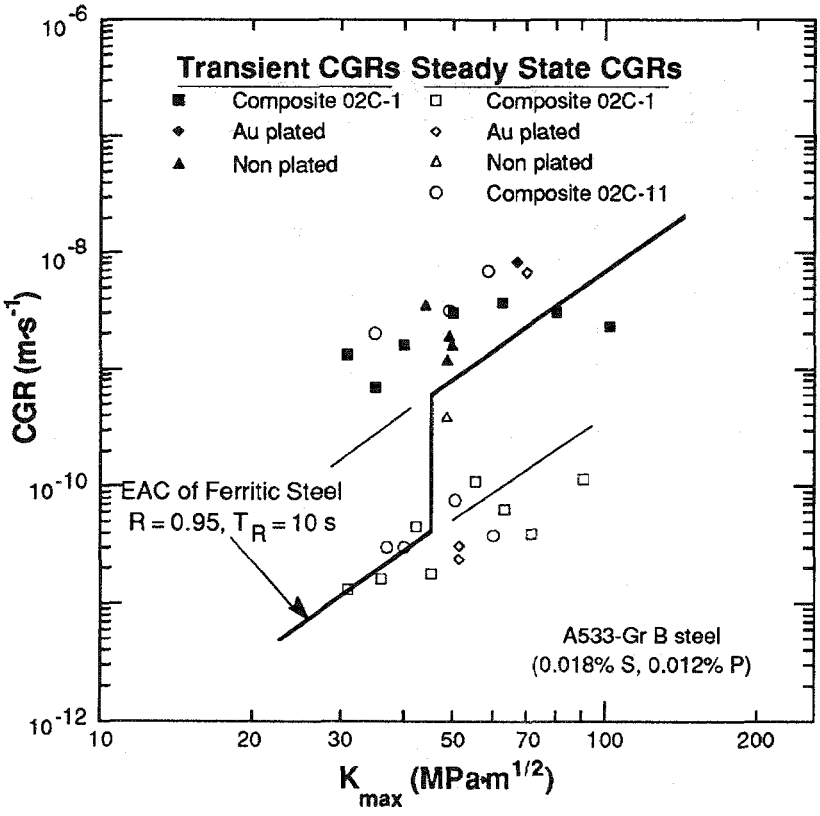

Figure 5. CGRs of A533–Gr B steel under R = 0.95 loading in HP oxygenated water at 289°C vs. K_{max}. Heavy line represents predicted behavior from a modified version of Section XI of the ASME code.

The upper–bound values for the experimental data in the high– and low–CGR regimes are ≈2 x 10^{-9} and 2 x 10^{-11} m·s^{-1} (≈2.5 and 0.025 in.·yr^{-1}), respectively, at a K_{max} value of 35 MPa·$m^{1/2}$. Crack–growth rates in the upper regime are clearly unacceptable. The nature of the transitions between the two regimes and the observation that the initial fatigue crack in companion nonplated specimens did not propagate will be investigated further in future experiments.

3.2.1 Crack–Growth–Rate Tests on Ferritic Steel Specimens (J. Y. Park)

In another autoclave system, CGR tests have begun on a set of three 1TCT carbon steel specimens [Nos. CTW7–03 (A533–Gr B Heat No. A5401, containing 0.004% S and 0.005% P); CTJ7–01 (A106–Gr B Heat No. J7201, containing 0.014% S and 0.014% P); and

02C-07 (A533-Gr B Heat No. A-1195-1, containing 0.018% S and 0.012% P)]. The chemical compositions of the steels are given in Table 1. Specimen No. 02C-07 was plated with nickel-chromium to simulate austenitic SS cladding on a pressure vessel steel and hence, determine the validity of using data obtained from specimens without cladding to analyze the behavior of a clad ferritic vessel where only the crack surface is exposed to the environment. In previous tests, gold- or nickel-plated specimens showed higher CGRs than a conventional specimen.

The tests were performed in deionized water at 289°C under a cyclic load (sawtooth wave shape with 12-s loading and 1-s unloading times) at an R value of 0.2, a frequency of 0.08 Hz, and a maximum initial stress intensity of 20 MPa·m$^{1/2}$. A dissolved-oxygen concentration of 200-300 ppb in the effluent water from the autoclave is maintained by feedwater containing 2-3 ppm oxygen. Crack length was measured by the DC potential-drop method. Results for the CGR tests are given in Table 6. The initial CGRs were 5.5 x 10^{-9}, 1.3 x 10^{-9} and 3.9 x 10^{-8} m·s^{-1}, for Specimens CTW7-03, CTJ7-01 and 02C-07, respectively. The maximum load was then increased by 25% and the tests were continued under the same load ratio and frequency. The CGRs increased to 1.0 x 10^{-8}, 3.3 x 10^{-8}, and 7.8 x 10^{-8} m·s^{-1} for respective specimens. The CGRs are plotted as a function of maximum stress intensity in Fig. 6. The line in the figure represents the new correlation submitted for inclusion in Section XI of the ASME code. Although the proposed Section XI curve is based almost solely upon data for pressure vessel steels, the data for the A106-Gr B piping steel appears to be consistent with the curve. The CGRs of all specimens are bounded by the ASME correlation. As expected, crack growth is faster in the nickel-chromium plated high-sulfur-content A533-Gr B steel. Because of crack growth, the K_{max} increased to 26, 28, and 42 MPa·m$^{1/2}$, for Specimens CTW7-03, CTJ7-01, and 02C-07, respectively. The tests are continuing under different load conditions.

Table 6. Crack Growth of A533-Gr B and A106-Gr B 1T-Compact Tension Specimens[a] at R = 0.2 Loading[b] in 289°C Water[c] Containing ≈200 ppb Dissolved Oxygen

			Electrode Potentials			A106-Gr B (No. CTJ7-01) Nonplated		A533-Gr B (No. 02C-07) Ni-Cr Plated		A533-Gr B (No. CTW7-03) Nonplated	
Test No.	Time, h	Cond., μS·cm^{-1}	A533-Gr B, mV(SHE)	Pt, mV(SHE)	Load Ratio	K_{max}[d], MPa·m$^{1/2}$	Growth Rate, m·s^{-1}	K_{max}[d], MPa·m$^{1/2}$	Growth Rate, m·s^{-1}	K_{max}[d], MPa·m$^{1/2}$	Growth Rate, m·s^{-1}
1	1012 1031	0.19	244	267	0.2	19.8	1.3 x 10^{-9}	23.1	3.9 x 10^{-8}	20.1	5.5 x 10^{-9}
2	1032 1049	0.19	255	263	0.2	28.3	3.2 x 10^{-8}	41.5	7.8 x 10^{-8}	26.3	1.0 x 10^{-8}

[a]Heat No. J7201 for A106 Gr-B (Specimen No. CTJ7-01), A-1195-1 for A533-Gr B (Specimen No. 02C-07) and A5401 for A533-Gr B (Specimen No. CTW7-03). Crack plane orientation was the L-T direction.

[b]Frequency of the positive sawtooth wave form was 8 x 10^{-2} Hz with a 12-s rise time.

[c]Effluent dissolved-oxygen concentration was ≈200-300 ppb; feedwater oxygen concentration was approximately one order of magnitude higher to compensate for oxygen depletion by corrosion of the autoclave system.

[d]Maximum stress intensity, K_{max}, values at the end of the time period.

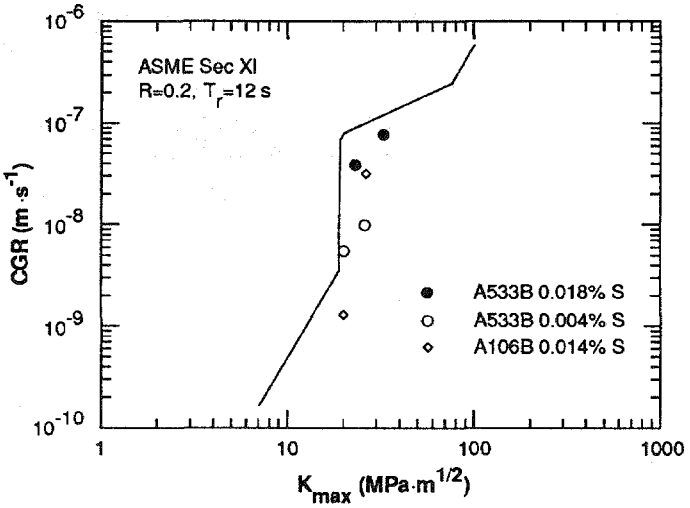

Figure 6. CGRs vs. K_{max} for A533–Gr B (0.004% S), Cr–Ni plated A533–Gr B (0.018% S), and A106–Gr B (0.014% S) specimens under R = 0.2 loading in HP oxygenated water at 289°C

4 SCC of Type 304 SS

4.1 Technical Progress

4.1.1 Role of Chromate and Sulfate in SCC of Type 304 SS (W. E. Ruther, W. K. Soppet, and T. F. Kassner)

Soluble corrosion products from system materials are the major species present in BWR water when ingress of ionic impurities into the coolant system from leaks in condenser tubes and from ion–exchange resins in the reactor water cleanup system (RWCS), including resin fines, is maintained at very low levels. Examples include Cu^+ and Cu^{2+} in plants with copper alloy condenser tubes and/or feedwater heaters and $HCrO_4^-$ from corrosion of SS piping, weld cladding on the interior of the reactor vessel, and internal components fabricated from this material. Although chromate (K_2CrO_4) is used as a corrosion inhibitor in component cooling water systems (CCWS) in BWRs and PWRs, these systems operate at relatively low temperatures (≈170°C) and pressures (≈150 psig); thus, direct ingress of chromate from the CCWS into the reactor coolant water is unlikely under normal operating conditions. Nevertheless, because only a small fraction of the recirculation water in BWRs passes through the RWCS, the concentration of corrosion–product ions in the reactor water can be considerably greater than in the feedwater (e.g., ≈25–35 ppb versus <1 ppb, respectively). Consequently, $HCrO_4^-$ and the counterbalancing hydronium cation (H_3O^+) are major contributors to water conductivity. To further mitigate IGSCC of sensitized Type 304 SS in these systems through water chemistry control, utilities have considered (1) neutralizing the residual chromic acid by NaOH additions to

the feedwater (to take advantage of the lower specific conductivity of Na^+ relative to that of H_3O^+), and (2) devising methods to remove chromate from the water by ion exchange.[22]

4.1.2 Experimental Methods

A fracture-mechanics CGR experiment was performed to determine the effect of chromate additions to simulated BWR water (without and with low levels of sulfate) on SCC of our reference heat (No. 30956) of Type 304 SS (composition is given in Table 1). Crack length was measured by the DC-potential-drop technique over time intervals of ≈800–1500 h at each test condition. Three specimens were heat treated to produce a solution-annealed condition and moderate and high levels of sensitization corresponding to electrochemical potentiokinetic reactivation (EPR) values of 0, 8, and 30 $C \cdot cm^{-2}$, respectively. The specimens were fatigue-precracked in HP water containing 200–300 ppb dissolved oxygen at 289°C. CGR tests were conducted in oxygenated water with different chromate and sulfate additions under several loading conditions.

4.1.3 Results

The water chemistry, loading conditions, and results of the CGR tests are given in Table 7. Steady-state CGRs were measured over time periods of ≈800–1200 h under each test condition. Baseline CGRs were determined under low-frequency (0.08 Hz), high-R (0.95) loading conditions in Tests 1 and 2 in Table 7. In Tests 3–6 and 9, either 0, 50, or 200 ppb chromate was added to the oxygenated feedwater and the CGRs were measured. In Tests 7, 8, 10, and 11, different concentrations of sulfate (between 6 and 100 ppb) were added to feedwater containing 50 ppb chromate to determine their combined effect on the CGRs of the steel. In Tests 12 and 13, the chromate concentration in the feedwater was increased to 200 ppb and the sulfate concentrations were 100 and 50 ppb, respectively.

The results in Table 7 reveal that the solution-annealed specimen (EPR = 0 $C \cdot cm^{-2}$) exhibited very low CGRs (<5 x 10^{-12} $m \cdot s^{-1}$) under all water chemistry conditions. Of the two sensitized specimens (EPR = 8 and 30 $C \cdot cm^{-2}$), the specimen with the lower EPR value exhibited the highest CGRs under each test condition. This level of sensitization produced maximum SCC susceptibility in slow-strain-rate-tensile (SSRT) tests at 289°C in oxygenated water without and with 100 ppb sulfate.[23] The results for the sensitized specimens can be summarized as follows. In oxygenated feedwater, 50–200 ppb chromate has a beneficial effect, as indicated by the low CGRs (<7 x 10^{-11} $m \cdot s^{-1}$) in Tests 3, 5, 6, and 9. In water containing 50 ppb chromate, low levels of sulfate (6 or 15 ppb) did not lead to high CGRs in Tests 10 and 11. In water containing 50 ppb chromate and 25 or 100 ppb sulfate (Tests 7 and 8), CGRs of the moderately sensitized specimen (EPR = 8 $C \cdot cm^{-2}$) increased significantly (to >3 x 10^{-10} $m \cdot s^{-1}$), whereas the heavily sensitized specimen exhibited this rate in water containing 100 ppb sulfate. At a higher chromate concentration (e.g., 200 ppb) in oxygenated feedwater containing 100 ppb sulfate (Test 12), the CGRs of the sensitized specimens were high (>1 x 10^{-10} $m \cdot s^{-1}$). However, after decreasing the sulfate concentration to 50 ppb (Test 13), the CGRs of the sensitized specimens decreased to <2 x 10^{-11} $m \cdot s^{-1}$.

Table 7. Crack Growth Results for Sensitized[a] Type 304 SS Specimens under High-R Loading[b] in High-Purity Oxygenated Water and in Oxygenated Water Containing Chromate and Sulfate at 289°C

Test No.	Test Time, h	Water Chemistry[c]				Electrode Potential		Material (Sensitization)					
		CrO_4^{2-} Conc.,[d] ppb	SO_4^{2-} Conc., ppb	Cond. at 25°C, μS·cm^{-1}	pH at 25°C	304 SS mV(SHE)	Pt mV(SHE)	304 SS (EPR = 0 C·cm^{-2}) K_{max}[e] MPa·m$^{1/2}$	304 SS (EPR = 0 C·cm^{-2}) Growth Rate, m·s^{-1}	304 SS (EPR = 8 C·cm^{-2}) K_{max}[e], MPa·m$^{1/2}$	304 SS (EPR = 8 C·cm^{-2}) Growth Rate, m·s^{-1}	304 SS (EPR = 30 C·cm^{-2}) K_{max}[e], MPa·m$^{1/2}$	304 SS (EPR = 30 C·cm^{-2}) Growth Rate, m·s^{-1}
1	0–300[c]	–	–	0.12	6.22	206	213	27.6	5×10^{-12}	29.2	9.2×10^{-10}	28.2	1.0×10^{-10}
2	300–1204	–	–	0.17	6.20	119	119	27.7	5×10^{-12}	30.9	3.3×10^{-10}	28.5	8.3×10^{-11}
3	1204–2350	50	–	0.30	6.21	67	58	27.7	5×10^{-12}	31.2	4.3×10^{-11}	28.5	8.7×10^{-12}
4	2350–3400	–	–	0.12	6.33	91	66	27.7	5×10^{-12}	31.5	4.3×10^{-11}	28.6	8.7×10^{-12}
5	3400–4400	200	–	0.82	5.81	80	80	27.7	5×10^{-12}	31.8	4.3×10^{-11}	28.7	8.7×10^{-12}
6	4400–5200	50	–	0.31	6.09	58	51	27.8	5×10^{-12}	31.8	4.3×10^{-11}	28.7	8.7×10^{-12}
7	5200–5900	50	25	0.46	6.01	91	96	27.8	5×10^{-12}	32.7	3.4×10^{-10}	28.7	8.7×10^{-12}
8	5900–7300	50	100	1.06	5.71	104	107	27.8	5×10^{-12}	35.3	4.1×10^{-10}	29.9	2.5×10^{-10}
9	7300–8800	50	–	0.27	6.15	86	71	27.8	9×10^{-13}	35.6	7.0×10^{-11}	30.0	3.6×10^{-11}
10	8800–10000	50	6	0.37	6.23	36	101	27.8	4×10^{-12}	35.7	2.3×10^{-11}	30.0	1.2×10^{-11}
11	10000–11200	50	15	0.44	6.09	37	107	27.9	6×10^{-12}	36.2	2.8×10^{-11}	30.1	1.1×10^{-11}
12	11200–11800	200	100	1.70	5.59	108	142	27.9	$<5 \times 10^{-12}$	37.9	3.0×10^{-10}	30.7	1.7×10^{-10}
13	11800–13000	200	50	1.32	5.66	14	39	27.9	$<5 \times 10^{-12}$	38.2	1.8×10^{-11}	30.9	1.8×10^{-11}

[a]Compact-tension specimens (1TCT) of Type 304 SS (Heat No. 30956) received a solution-anneal heat treatment at 1050°C for 0.5 h. Specimen No. 32 was tested in the solution-annealed condition (EPR = 0 C·cm^{-2}). Specimen No. 34 was sensitized at 700°C for 0.67 h (EPR= 8 C·cm^{-2}) and Specimen No. 33 at 700°C for 24 h (EPR = 30 C·cm^{-2}).

[b]Frequency and load ratio, R, for the positive sawtooth wave form were 8×10^{-2} Hz and 0.95, respectively.

[c]Effluent dissolved-oxygen concentration was ≈200–300 ppb, except in Test 1 at 5.5 ppm; feedwater oxygen concentration was higher by a factor of 3 in Tests 2–13 to compensate for oxygen depletion by corrosion of the autoclave system.

[d]Chromate and sulfate were added to the feedwater as acids; effluent chromate concentrations were ≈9 and 13 ppb for feedwater levels of 50 and 200 ppb on the basis of colorimetric analyses of grab samples.

[e]Maximum stress intensity, K_{max}, values at the end of the time period.

The present results indicate that the CGRs of the sensitized specimens may exhibit a unique dependence on sulfate and chromate concentrations in oxygenated feedwater. Figure 7 shows the CGRs of the moderately sensitized specimen (EPR = 8 C·cm^{-2}) as a function of the ratio of the concentrations of chromate and sulfate in the feedwater. When these species were not added to the feedwater (Table 7), their concentrations were assumed to be ≈1 ppb for the purpose of obtaining the ratios in Fig. 7. The limited data suggest that the CGRs are in the low regime if the $(CrO_4^{2-})/(SO_4^{2-})$ ratio in the feedwater is ≥3. Chromate concentrations in feedwater and effluent water were determined by colorimetric analyses (Cr^{+6}) on grab samples. The measured feedwater concentrations were in excellent agreement with the amounts added to the water; however, the effluent values were lower by a factor of >5 because of the low flow velocity and reaction with the large surface area of stainless steel in the autoclave system at 289°C. The feedwater and effluent sulfate concentrations were virtually the same in all experiments.

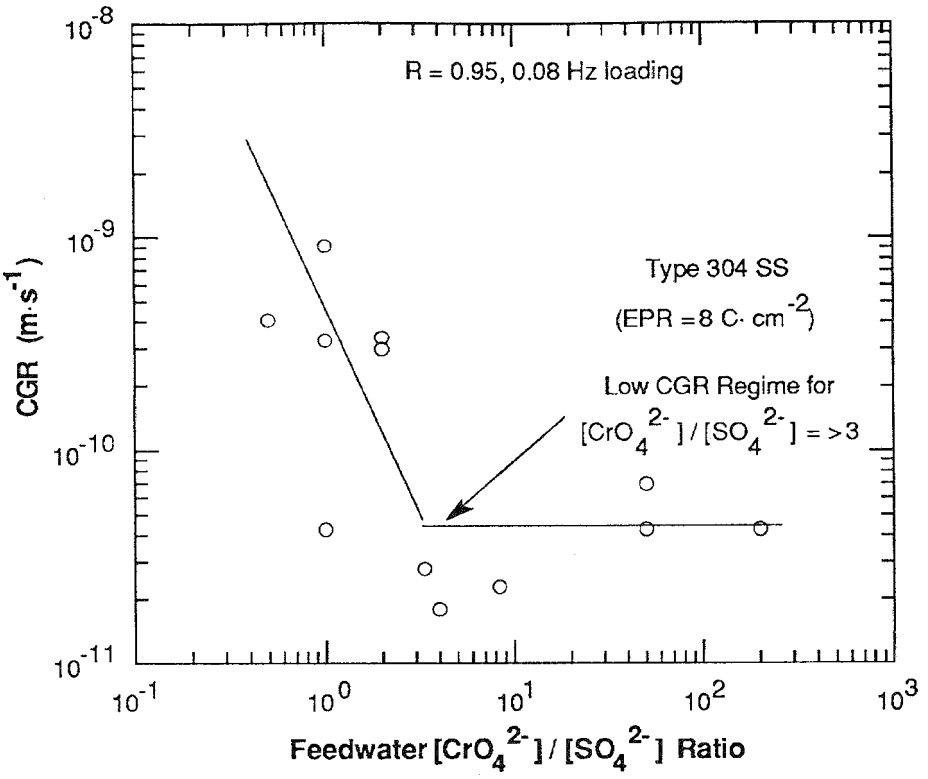

Figure 7. Regime of high and low CGRs for moderately sensitized (EPR= 8 C·cm^{-2}) Type 304 SS specimen at 289°C as a function of ratio of chromate and sulfate concentrations in feedwater containing ≈300 ppb dissolved oxygen

Although SSRT tests indicated that chromate at concentrations >100 ppb in oxygenated water contributes to IGSCC in a manner similar to that of other oxyanions,[22,24] the present CGR results suggest that this species has a mitigating effect on IGSCC at lower concentrations, provided that the sulfate concentration is lower by a factor of ≈3. Because chromate concentrations in BWR recirculation water are ≈25–35 ppb, the sulfate concentration should be maintained at <10 ppb to mitigate IGSCC. Achievable values for sulfate are <15 ppb and typically can be maintained at the ≈5 ppb level. Consequently, these water chemistry conditions would place sensitized Type 304 SS in the low-CGR regime. Efforts to remove chromate from recirculation loop water without decreasing the critical sulfate level could be counterproductive. Furthermore, maintaining sulfate concentrations at levels of <5 ppb may be impractical.

5 Irradiation-Assisted Stress Corrosion Cracking of Austenitic SS

5.1 Technical Progress

5.1.1 Slow-Strain-Rate Tests on Irradiated Austenitic SS (H. M. Chung, W. E. Ruther, and A. G. Hins)

In recent years, failures of reactor-core internal components in both BWRs and PWRs have increased after accumulation of relatively high fluence (>5 x 10^{20} n·cm^{-2}, E >1 MeV). The general pattern of the observed failures indicates that as nuclear plants age and neutron fluence increases, various apparently nonsensitized austenitic materials become susceptible to intergranular failure. Some components are known to have cracked under minimal applied stress. Although most failed components can be replaced, some safety-significant structural components, such as the BWR top guide, shroud, and core plate, would be very difficult or impractical to replace. Therefore, the structural integrity of these components after accumulation of high fluence has been a subject of concern, and extensive research has been conducted to provide an understanding of this type of degradation, which is commonly known as irradiation-assisted stress corrosion cracking (IASCC).[25-42]

Most of the safety-significant structural components are fabricated from solution-annealed austenitic SSs, primarily commercial-purity Type 304 SS. Component fabrication procedures and reactor operational parameters, such as neutron flux, fluence, temperature, water chemistry, residual stress, and mechanical loads, have been reported to influence susceptibility to IASCC.[25-36] However, results from research at several laboratories on materials irradiated under a wide variety of simulated conditions are often inconsistent and conflicting as to the influence of these parameters.[28,35]

Failures of austenitic SS after accumulation of high fluence have been attributed to irradiation-induced segregation (RIS) or depletion of elements such as Si, P, S, Ni, and Cr at grain boundaries. It is generally believed that the nonequilibrium process of RIS of impurity or alloying elements is strongly influenced by irradiation temperature and fast-neutron dose rate. However, the exact identity of the elements that segregate and the extent to which RIS contributes to the enhanced susceptibility of the core-internal components of LWRs to IASCC are not clear. This is particularly true for Type 304 SS, from which the majority of the safety-significant in-core components have been fabricated, although analyses of RIS of impurity elements and grain-boundary depletion of Cr have been reported for Type 304 SS specimens irradiated under simulated conditions, i.e., either in test reactors,[29,30,32] by electrons,[29] or ions.[34,36]

In view of the strong influence of irradiation temperature and dose rate, results obtained from specimens irradiated in test reactors and accelerators must be considered as tentative, and benchmark analyses on actual reactor components must be obtained. For this purpose, high- and commercial-purity (HP and CP) Type 304 SS specimens obtained from neutron absorber tubes of two operating BWRs were analyzed by Auger electron spectroscopy (AES) previously.[40,41] HP Type 304 SS has been suggested as an alternative to CP Type 304 SS. In-reactor and laboratory experience[26,27,33] indicate better IASCC

performance of an HP heat of Type 348 SS than of a CP heat of Type 348 SS. Auger analyses of specimens from a CP Type 304 SS neutron absorber rod revealed significant segregation of Si, P, Ni, and an unidentified element or compound that gives rise to an Auger energy peak at 59 eV.[40,41] Such segregation was negligible in HP material, except for Ni. No evidence of S segregation was observed in either material. However, Cr depletion was more pronounced in the HP material than in the CP material.

The results of the AES analyses of irradiation-induced grain-boundary segregation of impurity and alloying elements have been correlated with SCC susceptibility information from SSRT tests on specimens from neutron-absorber-rod tubes to provide insight into mechanism(s) of IASCC.

5.1.2 Experimental Methods

Procedures for preparation of the slow-strain-rate-tensile (SSRT) test specimens and a description of the hot-cell SSRT apparatus were given in a previous report.[41] The SSRT specimens (89 mm long) were sectioned from top-, middle-, and bottom-axial positions of the neutron-absorber-rod tubes. Maximum fluence at the top was determined from known in-reactor flux data. Lower fluences at the other two axial locations were determined from results of ^{60}Co gamma scans on the entire length of the rods. The relative fluence of each 89-mm-long SSRT specimen and the needlelike AES specimens was verified further by measuring gamma activity of each specimen after the boron carbide neutron absorber was removed from the absorber-rod tubes.[41] The fluence levels and chemical compositions of the HP and CP specimens are given in Table 8. Documents on the chemical composition of the as-fabricated neutron absorber of the CP grade were not available from either the utility or the reactor-fuel supplier; therefore, the composition of the CP heat was determined after discharge from the reactor following several years of service.

SSRT tests were conducted on 12 specimens of CP and HP neutron-absorber-rod tubes in air and in simulated BWR water at 289°C at a strain rate of 1.65×10^{-7} s^{-1} to determine tensile properties and IASCC susceptibility as a function of neutron fluence. The dissolved-oxygen concentration and conductivity of the simulated BWR water were ≈280 ppb and 0.13 $\mu S \cdot cm^{-1}$, respectively. SEM fracture surface maps of the SSRT specimens were also obtained. SEM fractography was conducted at a magnification of 125X, and an entire fracture-surface composite was constructed for each specimen to determine the fraction of intergranular, transgranular, and ductile failure.

Table 8. Chemical Composition and Fast-Neutron Fluence of Irradiated Type 304 SS BWR Absorber-Rod Cladding

Material	Fluence Level,	Specimen Code	Composition (wt.%)									
	10^{21} n·cm^{-2}		Cr	Ni	Mn	C	N	B	Si	P	S	O
HP-304 SS[a]	1.4	VH-A7A	18.50	9.45	1.53	0.018	0.100	<0.001	<0.03	0.005	0.003	-
HP-304 SS[a]	0.7	VM-D5B	18.58	9.44	1.22	0.017	0.037	0.0002	0.02	0.002	0.003	-
HP-304 SS[a]	0.2	VL-A4C			same	as	VH-	A7A				
CP-304 SS[b]	2.0	BL-BWR-2H	16.80	8.77	1.65	0.08[c]	0.052	-	1.55	0.045[c]	0.030[c]	0.024
	0.6	BL-BWR-2M										
	0.2	BL-BWR-2L										

[a]HP neutron-absorber tubes, 4.78-mm-OD, 0.63-mm-wall; composition measured before service.
[b]CP neutron-absorber tube, 4.78-mm-OD, 0.79-mm-wall; composition measured after service.
[c]Represents maximum value in the specification; actual value not measured.

5.1.3 Results

Test conditions, SSRT data, and SEM analyses of the 12 specimens are summarized in Table 9. Stress versus elongation curves for the CP and HP specimens are shown in Figs. 8 and 9, respectively. Each figure portrays SSRT data for low-, medium-, and high-fluence specimens strained to failure in simulated BWR water and air. Because the cross-sectional area of the pull rod is large compared to that of the absorber tube specimen, the internal pressure in the autoclave produces a high initial stress (240 to 290 MPa) on the specimens tested in water. However, the relative characteristics of stress corrosion of the HP and CP specimens can be deduced from these figures. As fluence increases, the relative reduction in elongation (namely, the ratio of elongation in water to that in air) becomes smaller, indicating a greater degree of SCC. For a comparable fluence level of $\approx 0.7 \times 10^{21}$ n·cm^{-2} (Figs. 8B and 9B), the total elongation of the HP specimen tested in the simulated BWR water (≈2%) was significantly lower than that of the CP specimen (≈6.7%).

Table 9. Slow-Strain-Rate-Tensile[a] Test Results on Irradiated CP and HP Type 304 SS in Air and in HP Water Containing ≈280 ppb Dissolved Oxygen at 289°C

Absorber Rod Specimen No.	Hot-Cell Identification No.	Fast-Neutron Fluence, n·cm^{-2}	SSRT No.	Feedwater Chemistry			SSRT Parameters				
				Oxygen Conc., ppb	Cond. at 25°C, μS·cm^{-1}	pH at 25°C	Failure Time, h	Maximum Stress, MPa	Total Elong., %	TGSCC, %	IGSCC, %
BL-BWR-2H	389E3A	2.0×10^{21}	IR-9	b	b	b	228	631	13.5	0	0
BL-BWR-2H	389E3D	2.0×10^{21}	IR-12	300	0.13	6.27	21	415	1.2	8	28
BL-BWR-2M	389E2D	0.6×10^{21}	IR-3	b	b	b	580	465	34.8	0	0
BL-BWR-2M	389E2A	0.6×10^{21}	IR-8	290	0.15	6.32	140	359	8.3	55	0
BL-BWR-2L	389E1A	0.2×10^{21}	IR-2	b	b	b	260	390	15.6	0	0
BL-BWR-2L	389E1D	0.2×10^{21}	IR-1	280	0.13	6.23	107	337	6.7	43	0
VH-A7A-L2	406A1F	1.4×10^{21}	IR-5	b	b	b	93	786	5.6	0	0
VH-A7A-L1	406A1E	1.4×10^{21}	IR-4	280	0.10	6.28	11	417	0.6	2	58
VM-D5B-L2	406C3	0.7×10^{21}	IR-6	b	b	b	405	684	24.2	-	-
VM-D5B-L1	406C2	0.7×10^{21}	IR-7	280	0.12	6.26	31	552	1.8	8	34
VL-A4C-L2	406B3	0.2×10^{21}	IR-10	b	b	b	231	607	13.7	-	-
VL-A4C-L1	406B2	0.2×10^{21}	IR-11	330	0.14	6.33	77	520	4.6	47	14

[a]Strain rate of 1.65×10^{-7} s^{-1}.

[b]Test in air at 289°C and strain rate of 1.65×10^{-7} s^{-1}.

5.1.3.1 Tensile Properties

Tensile properties of the CP- and HP-grade neutron-absorber tubes, obtained from the specimens tested in air, were significantly modified as neutron fluence increased to $>0.5 \times 10^{21}$ n·cm^{-2}. Figures 10 and 11 show the yield strength (YS) and ultimate tensile strength (UTS) versus fast-neutron fluence (E >1 MeV) of the CP and HP specimens strained to failure in air (from Table 9). The figures contain similar data for CP-grade BWR plate[25] and CP-grade tensile specimens of Types 304 and 304L SS irradiated in the Advanced Test Reactor (ATR) at 300°C.[30]

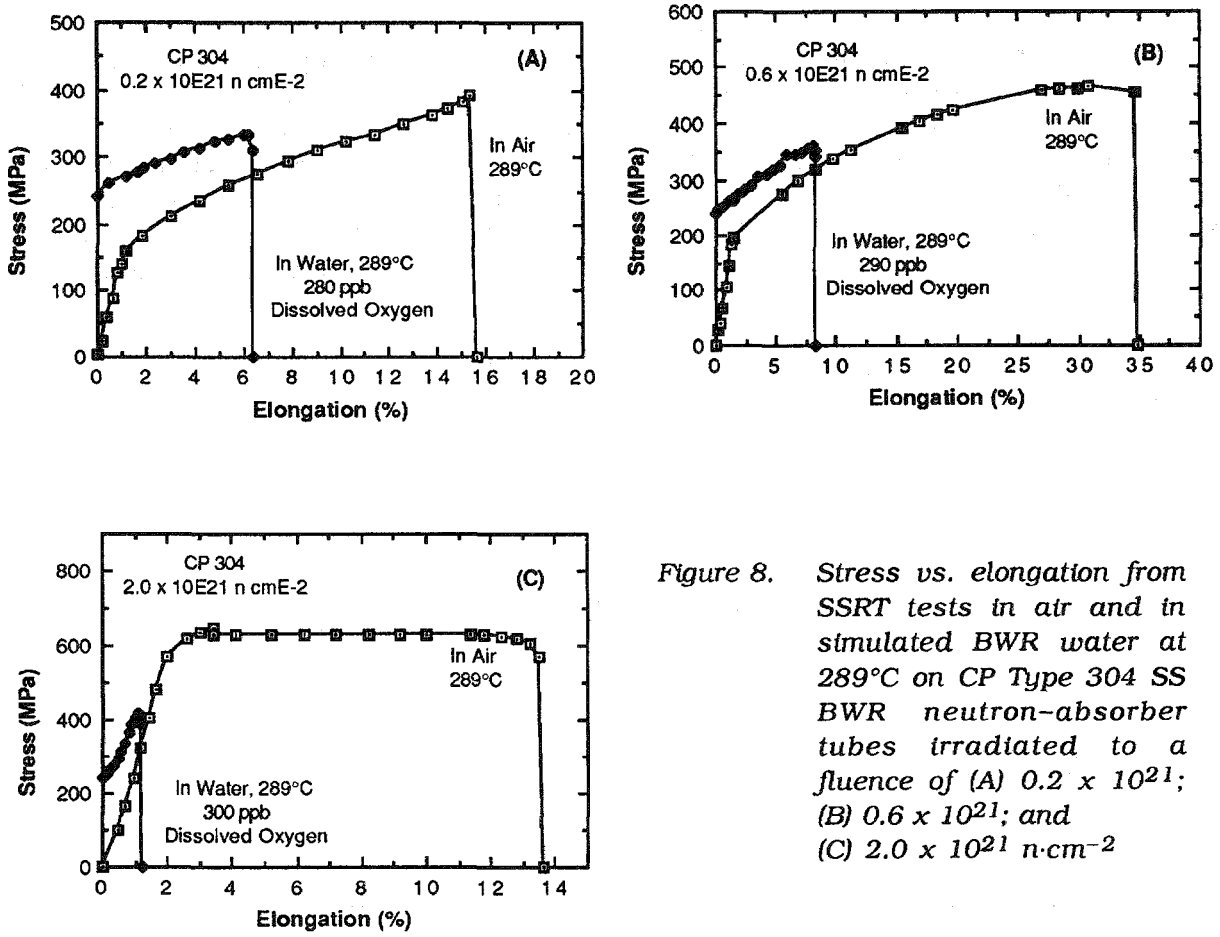

Figure 8. Stress vs. elongation from SSRT tests in air and in simulated BWR water at 289°C on CP Type 304 SS BWR neutron-absorber tubes irradiated to a fluence of (A) 0.2 x 10^{21}; (B) 0.6 x 10^{21}; and (C) 2.0 x 10^{21} n·cm^{-2}

Both YS and UTS data obtained from the present CP neutron-absorber tube are consistent with those of the CP materials reported by Clarke and Jacobs[25] and Jacobs et al.[30] The YS and UTS of the CP materials increase by a factor of ≈4 and 2, respectively, as fluence increases from 0 to 3 x 10^{21} n·cm^{-2}. However, for a comparable fluence level, both the YS and UTS of the HP neutron-absorber tube are significantly higher than those of the CP materials. Fracture surfaces of the present CP and HP specimens were examined by SEM to characterize the morphologies. The ductile-dimple fracture morphologies in the CP and HP specimens were somewhat different, and tear ridges were observed only in the CP material. However, based on SEM fractography, it was not clear why the strength of the HP heat was higher than that of the CP heat. To obtain a better understanding of relative microstructural characteristics of the two heats, TEM examination is planned. No evidence of intergranular morphology was observed in the fracture surfaces of the HP and CP specimens strained to failure in air.

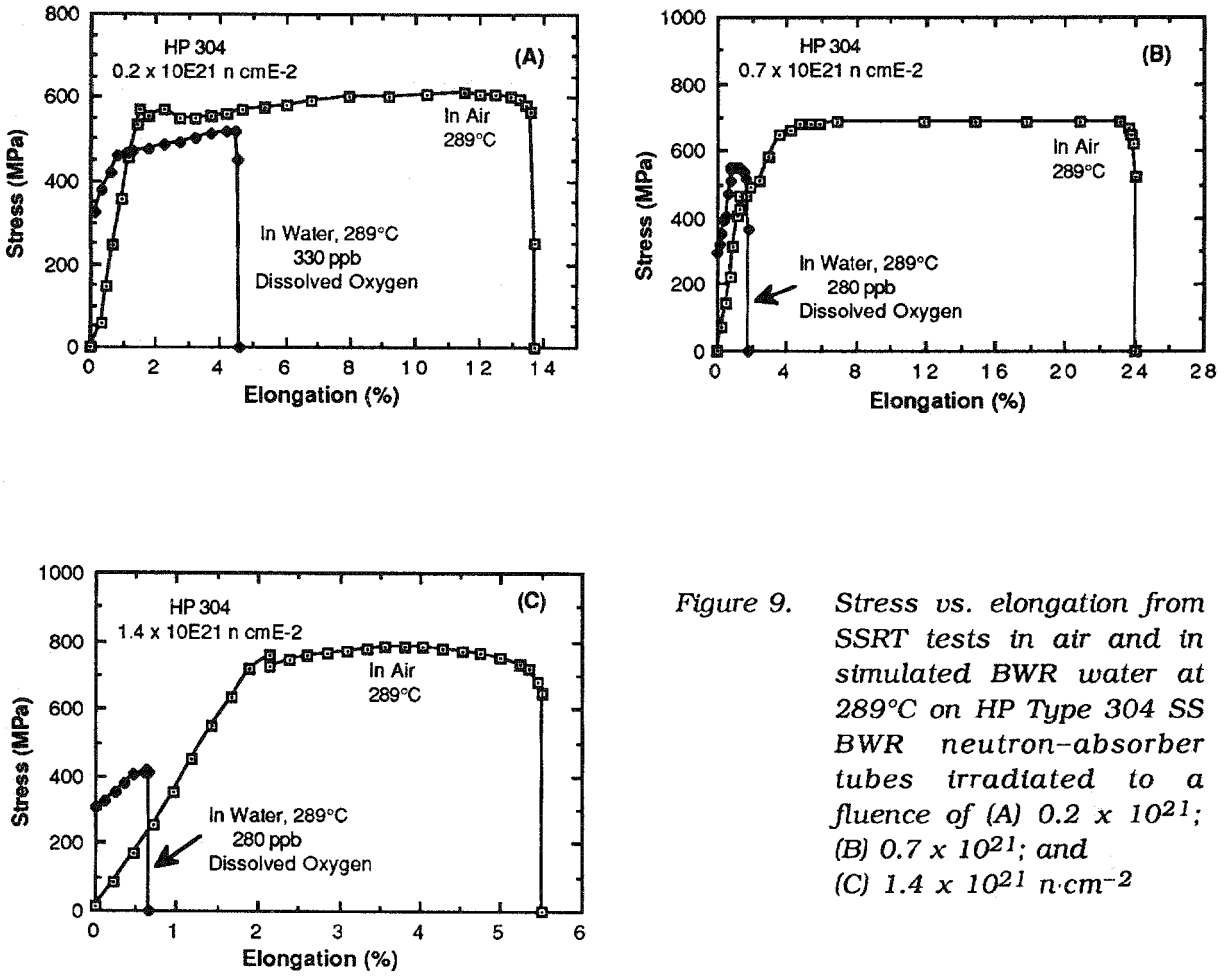

Figure 9. Stress vs. elongation from SSRT tests in air and in simulated BWR water at 289°C on HP Type 304 SS BWR neutron-absorber tubes irradiated to a fluence of (A) 0.2 x 10^{21}; (B) 0.7 x 10^{21}; and (C) 1.4 x 10^{21} n·cm^{-2}

Figure 12 shows the total elongation versus fast-neutron fluence for the HP and CP materials. For comparison, similar data from Refs. 25 and 30 for CP heats of Type 304 and 304L SS are also shown in the figure. The latter data were obtained at a significantly higher strain rate than that in the present tensile tests, i.e., 4 x 10^{-4} s^{-1} versus 1.7 x 10^{-7} s^{-1}. Despite the differences in strain rate and composition (i.e., HP vs. CP), the effects of fluence on total elongation of both heats seem to be essentially the same. This is in contrast to the effect of fluence on strength. Ductility appears to reach an asymptotic minimum value of ≈5% at fluence levels >1.5 x 10^{21} n·cm^{-2}.

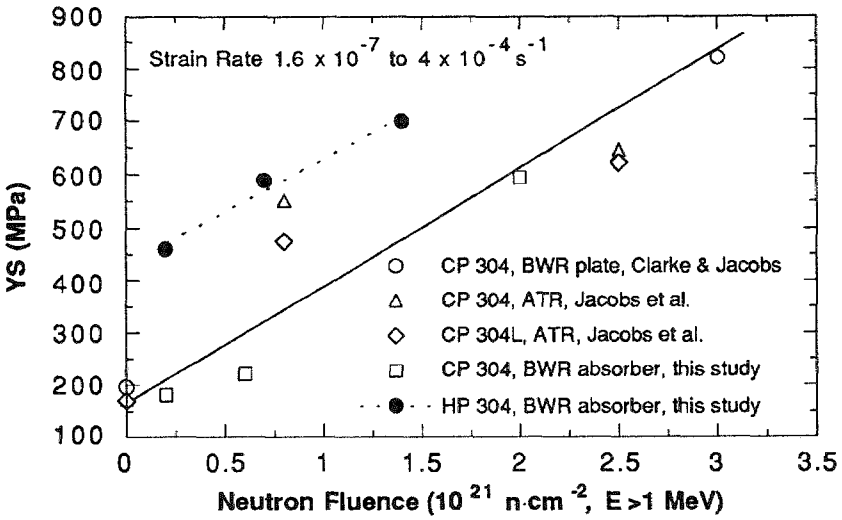

Figure 10. Yield stress vs. fast neutron fluence (E >1 MeV) for solution-annealed CP and HP Type 304 SS from tensile tests in air at 289°C

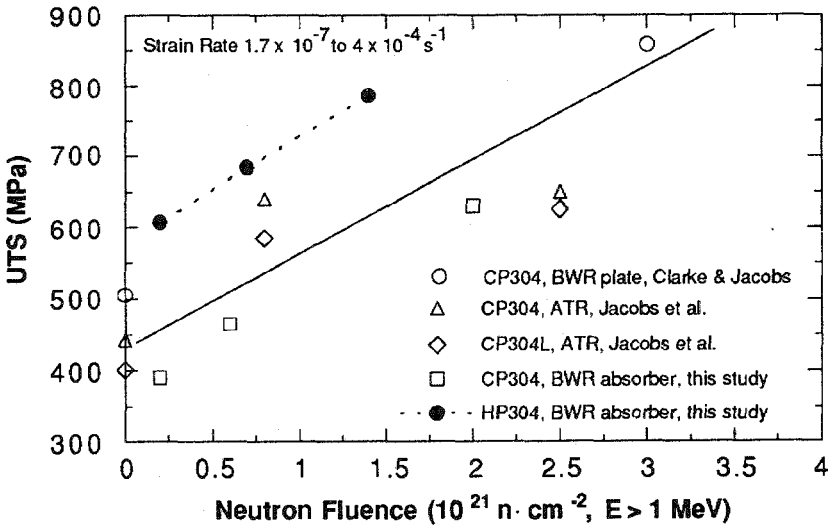

Figure 11. Ultimate tensile stress (UTS) vs. fast-neutron fluence (E >1 MeV) for solution-annealed CP and HP Type 304 SS from tensile tests in air at 289°C

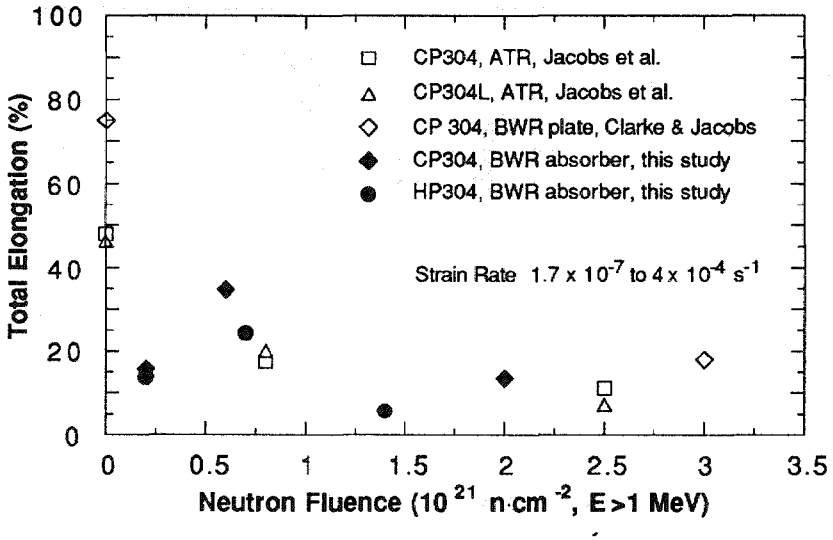

Figure 12. Total elongation vs. fast-neutron fluence (E >1 MeV) for solution-annealed CP and HP Type 304 SS from tensile tests in air at 289°C

5.1.3.2 SCC Susceptibility

A comparison of the stress versus elongation curves (Fig. 13) for the HP and CP specimens strained to failure in simulated BWR water reveals the relative susceptibility of the materials to SCC. At all fluence levels, the total elongations of the HP material were lower than those of the CP heat, indicating a higher SCC susceptibility of the HP material. For example, at a fluence level of 0.6 to 0.7 x 10^{21} n·cm^{-2} (Fig. 13B) the total elongation of the HP specimen was ≈1.8%, compared to ≈8.3% for the CP specimen.

To determine SCC susceptibilities more quantitatively, SEM micrographs of the fracture surfaces of the HP and CP specimens were obtained at a magnification of 125X. Fracture maps that depict regions of intergranular (IG), transgranular (TG), and ductile fracture for three HP and CP specimens are shown in Fig. 14(A-F). The fractions of IG and TG fracture, i.e., percent IGSCC and TGSCC, respectively, were measured from the composite fracture surface maps and results were given in Table 9. The HP and CP specimens irradiated to a fluence of 0.6 to 0.7 x 10^{21} n·cm^{-2} exhibited ≈34 and 0% IGSCC, respectively, which is consistent with the lower total elongation of the HP specimen [Fig. 13(B)], i.e., ≈1.8 vs. 8.3 %, respectively. The HP specimen irradiated to a fluence of 1.4 x 10^{21} n·cm^{-2} (Fig. 13C) exhibited IG fracture on ≈58% of the fracture surface [Fig. 14(C)]. Based on the maximum depth of IG fracture from the surface map and time to failure, the CGR in this specimen is ≈1.6 x 10^{-8} m·s^{-1}. This rate is virtually the same as that for sensitized Type 304 SS from SSRT tests on cylindrical specimens in oxygenated water at a low strain rate.[43-45] The CGR of the HP specimen is higher by factor of ≈10 than that of the CP specimen irradiated to a fluence of 0.2 x 10^{21} n·cm^{-2} [Fig. 13(A)], in which

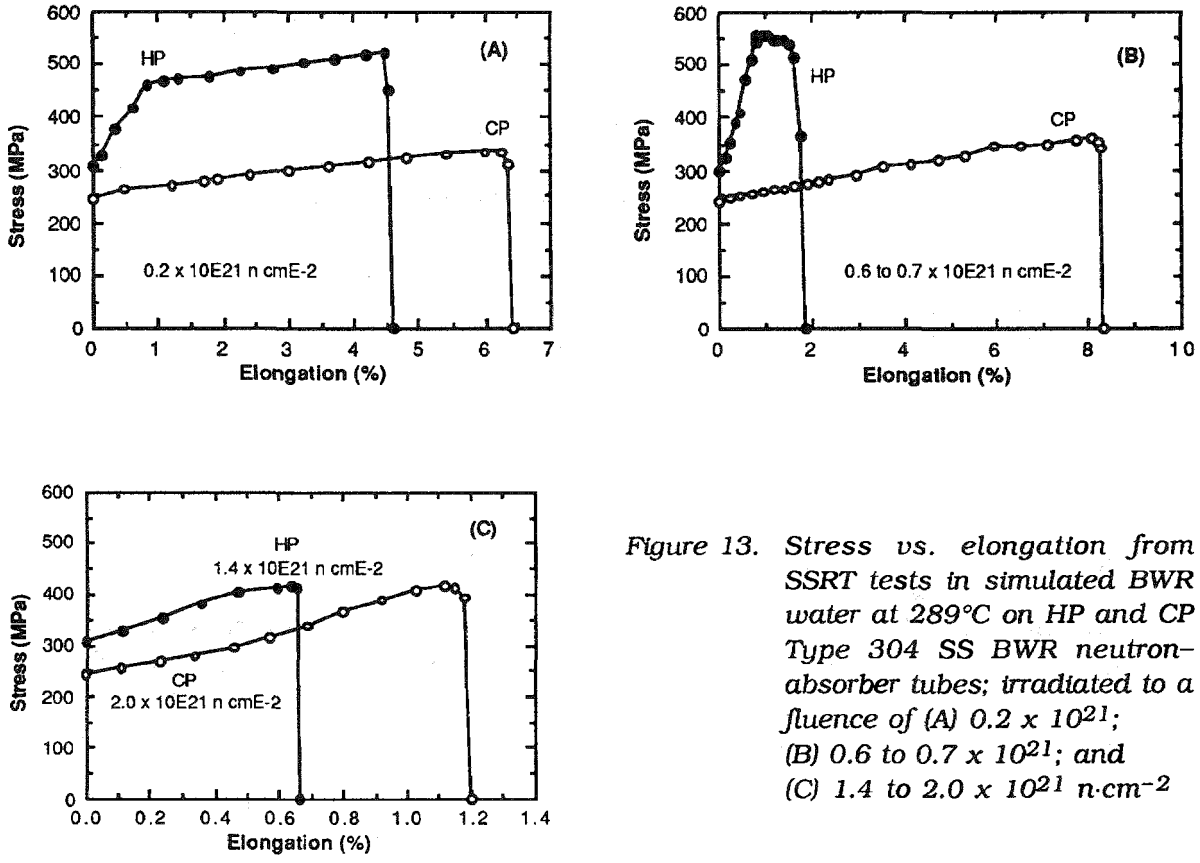

Figure 13. Stress vs. elongation from SSRT tests in simulated BWR water at 289°C on HP and CP Type 304 SS BWR neutron-absorber tubes; irradiated to a fluence of (A) 0.2 x 10^{21}; (B) 0.6 to 0.7 x 10^{21}; and (C) 1.4 to 2.0 x 10^{21} n·cm^{-2}

the fracture mode was predominantly TG and ductile failure [Fig. 14(D)]. Typical IG fracture morphologies for HP and CP specimens irradiated to the highest fluence levels (1.4 to 2.0 x 10^{21} n·cm^{-2}) are shown in Figs. 15 (A) and (B), respectively.

For the three HP and CP SSRT specimens tested in simulated BWR water, the percent IGSCC determined from SEM fractography was, in general, consistent with the decrease in total elongation. This is shown in Fig. 16. The total elongation values were corrected (increased) to account for the initial elongation caused by the stress exerted on the specimens in high-pressure water before the mechanical load was applied (Figs. 8 and 9). Literature data from SSRT tests on Types 304 and 316 SS from CP-grade BWR components are also plotted. The figure indicates that total elongation is also a good measure of IGSCC susceptibility.

Figure 17 shows a relationship between the percent IGSCC and neutron fluence for our CP heat of Type 304 SS, along with similar data of Clark and Jacobs,[25] Jacobs et al.,[30] and Kodama et al.[42] on CP heats of Types 304 and 316 SS. The materials in the study by Jacobs et al.[30] were irradiated at 300°C in the ATR, whereas the other heats were from BWR-irradiated components. The SSRT tests in all of the studies were conducted at 288 or 289°C in simulated BWR water containing several dissolved-oxygen concentrations, namely, 0.2, 8, or 32 ppm. Despite the wide range of strain rates and dissolved-oxygen

concentrations in the various tests, the dependence of IG fracture morphology (percent IGSCC) on neutron fluence is reasonably consistent.

A comparison of the percent IGSCC versus fast-neutron fluence (E >1 MeV) for the present CP and HP heats is shown in Fig. 18, along with similar results from SSRT tests on CP grade BWR dry tubes reported by Kodama et al.[42] All of these data were obtained at a strain rate of $\approx 2 \times 10^{-7}$ m·s^{-1} in water containing ≈200 ppb dissolved oxygen. The figure indicates that IGSCC susceptibility of CP material from our neutron-absorber tube and the dry tube is similar at a comparable fluence level, and that the HP material exhibits greater SCC susceptibility. Duplicate tests will be performed on specimens from the HP-grade absorber tube and the CP-grade control-blade-sheath to further confirm the results.

6 Summary of Results

6.1 Fatigue of Ferritic Piping and Pressure Vessel Steels

- The fatigue lives of a medium-sulfur-content A533-Gr B pressure vessel and A106-Gr B piping steels were studied in high-purity deoxygenated water, in simulated PWR water, and in air. Compared to results in air, the lives of A533-Gr B steel in water in most cases were shorter by a factor of ≈2. One test at a slower strain rate (by a factor of 100) indicated that strain rate has a minimal effect on fatigue life in deoxygenated water. No significant effect of the environment was observed in tests on A106-Gr B steel.

6.2 Stress Corrosion Cracking of Ferritic Steels

- Fracture-mechanics CGR tests have been performed on composite specimens of A533-Gr B/Inconel-182/Inconel-600 plated with nickel, and on homogeneous specimens of A533-Gr B material plated with gold and nickel. The effects of load history and dissolved-oxygen content were examined. The CGRs increased markedly during small-amplitude cyclic loading (R = 0.95). Under the cyclic loading, crack growth was observed at K_{max} values that produced no crack growth under constant (R = 1) loading. Under R = 0.95 loading, relatively high CGRs (2×10^{-9} m·s^{-1}) were observed in HP water containing ≈300 ppb dissolved oxygen. When the specimen is in the low-CGR regime (2×10^{-11} m·s^{-1}), increasing the dissolved-oxygen concentration to 6 ppm or higher initiated a return to the high CGR regime, at least at an R value of 0.95.

6.3 Effects of Chromate and Sulfate on SCC of Type 304 SS

- Current BWR operating practices have reduced to very low levels the ingress of ionic impurities (e.g., sulfate, chloride) into the coolant system. Soluble corrosion products viz., chromate and the counterbalancing hydronium ion, are now the major ionic

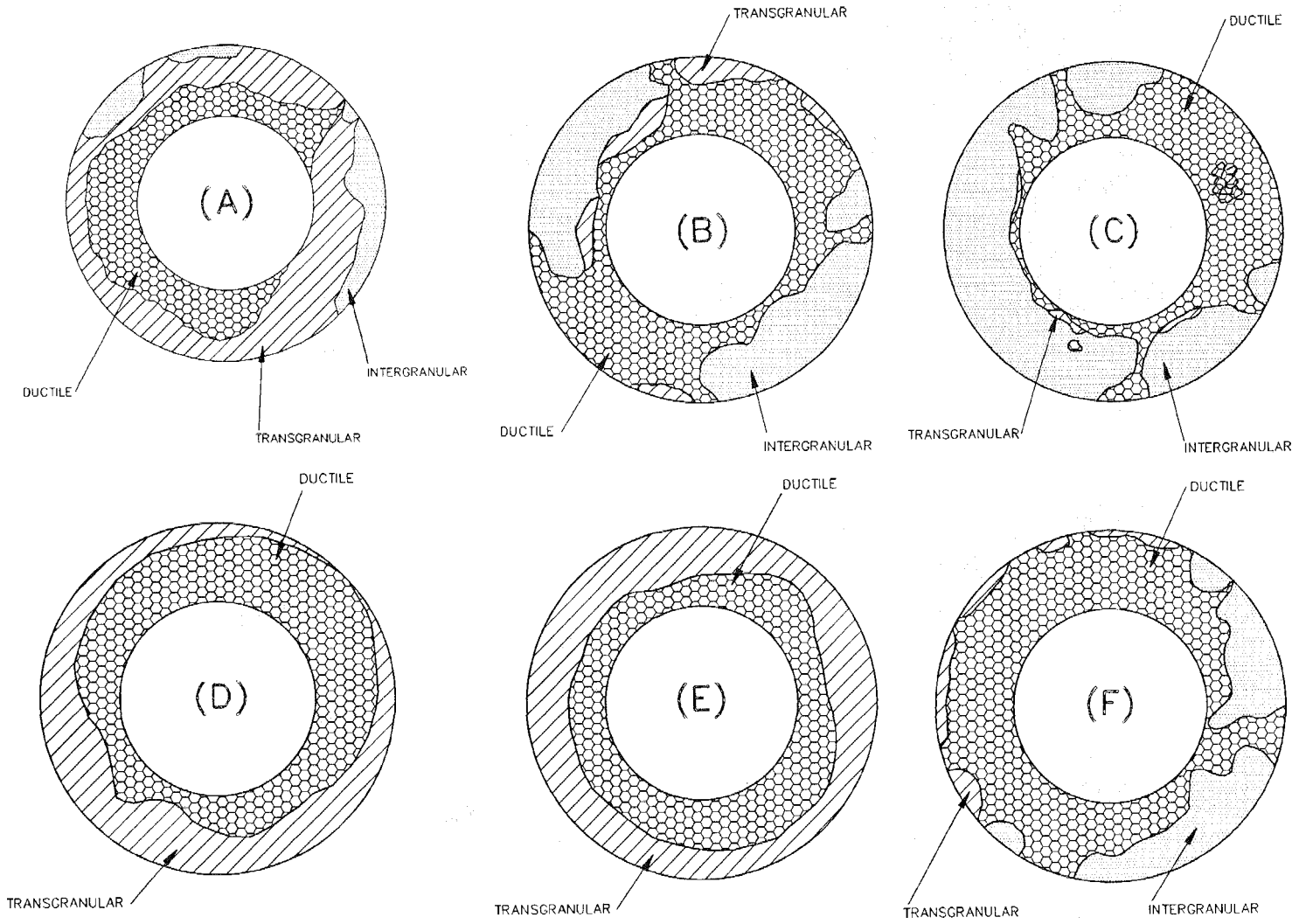

Figure 14. Schematic of composite fracture surface morphologies of irradiated SSRT specimens strained to failure in simulated BWR water: HP specimens irradiated to fluence levels of (A) 0.2 x 10^{21}; (B) 0.7 x 10^{21}; and (C) 1.4 x 10^{21} n·cm^{-2}; and CP specimens to (D) 0.2 x 10^{21}; (E) 0.6 x 10^{21}; (F) 2.0 x 10^{21} n·cm^{-2}

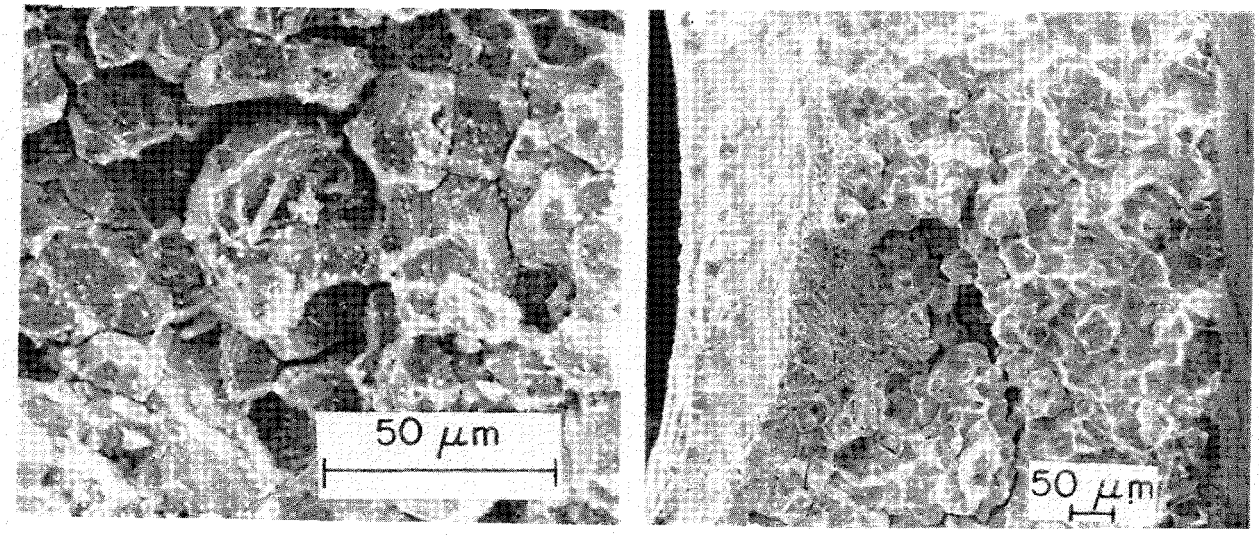

Figure 15. Intergranular fracture surface morphologies of high-fluence specimens of Type 304 SS depicted in Fig. 14(C) and (F); HP (left) and CP (right), respectively

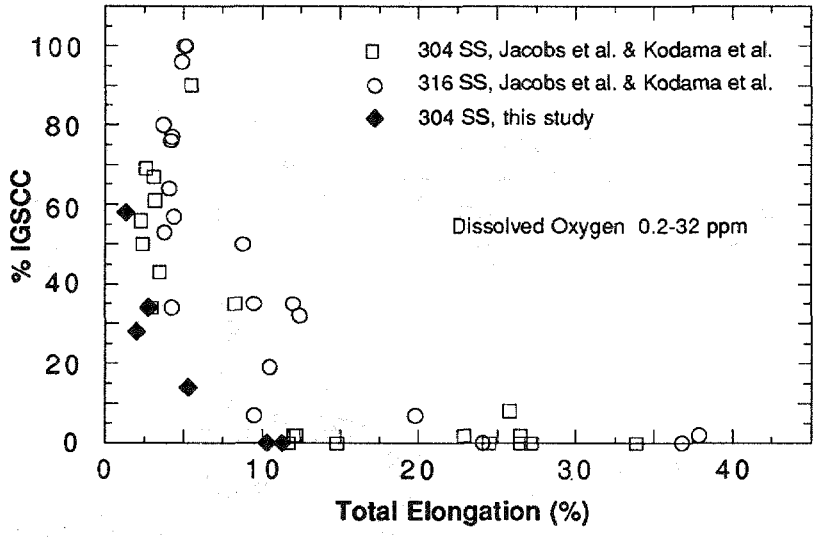

Figure 16. Percent IGSCC vs. total elongation of CP and HP Type 304 SS in the present study and similar data from the literature[30,32,33,42] from SSRT tests at 288°C in simulated BWR water containing 0.2 to 32 ppm dissolved oxygen

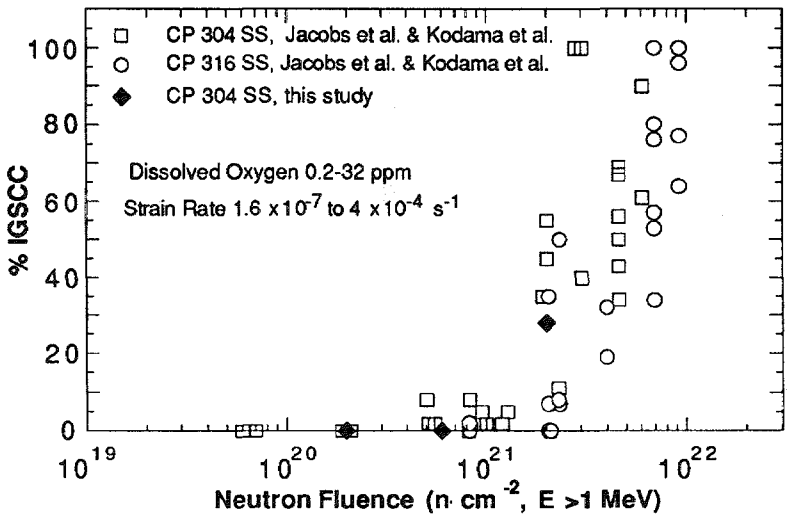

Figure 17. Percent IGSCC vs. fast-neutron fluence (E >1 MeV) for CP Type 304 and 316 SS from SSRT tests at 288–289°C in simulated BWR water containing 0.2–32 ppm dissolved oxygen

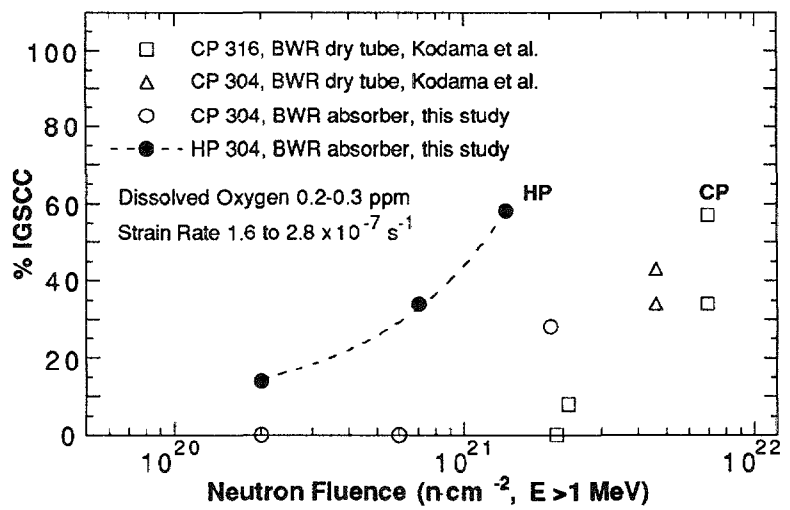

Figure 18. Percent IGSCC vs. fast-neutron fluence (E >1 MeV) for HP Type 304 SS and CP Type 304 and 316 SS[42] from SSRT tests at 288°C in simulated BWR water containing 200–300 ppb dissolved oxygen. HP material exhibits higher susceptibility than CP heats.

species present. Because only a small fraction of the recirculation water in BWRs passes through the reactor water cleanup system, the concentration of chromate ions in the reactor water can be much greater than in the feedwater (e.g., ≈25–35 ppb versus <1 ppb, respectively). The CGRs of sensitized Type 304 SS under high–R, low–frequency loading are low (<4 x 10^{-11} m·s^{-1}) provided that the chromate/sulfate concentration ratio in oxygenated feedwater is >3. Thus, a low chromate concentration in BWR water (25–35 ppb) may actually have a beneficial effect on SCC, provided that the sulfate concentration is below a critical level (i.e., ≈10 ppb).

6.4 Irradiation–Assisted Stress Corrosion Cracking of Type 304 SS

- Failures of austenitic SS after accumulation of high fluence have been attributed to radiation–induced segregation (RIS) of elements such as Si, P, S, Ni, and Cr. Microchemical and microstructural changes in high– and commercial–purity (HP and CP) Type 304 SS specimens from control–blade absorber tubes in two operating BWRs were studied by Auger electron spectroscopy and SEM. SSRT tests were conducted on tubular specimens in air and in simulated BWR water at 289°C. Results in air showed that the yield and ultimate tensile strengths of the HP material were higher than those of the CP material for a comparable fluence.

- Stress versus elongation characteristics of the SSRT specimens were consistent with results of SEM analyses of the percent IGSCC on fracture surfaces. IGSCC susceptibility of the present CP absorber tubes was similar to that of other CP heats of Types 304 and 316 SS reported in the literature. However, the HP absorber tubes exhibited greater IGSCC susceptibility than did the CP materials.

- It is difficult to explain the relatively high susceptibility of the HP material on the basis of Si or P segregation, because impurity segregation in the HP absorber tubes was negligible for all fluence levels. Rather, the high susceptibility seems to be consistent with the observation that irradiation–induced Cr depletion was more significant in the HP heat than in the CP heat, indicating that irradiation–induced grain–boundary depletion of Cr is the primary process in IASCC, at least in simulated BWR water.

Acknowledgments

W. F. Burke, D. R. Perkins, J. E. Sanecki, G. J. Talaber, and J. C. Tezak contributed to the experimental effort in this program. This work was conducted in programs titled "Environmentally Assisted Cracking in LWR Systems" and "Materials Studies on Service Aged Components" and sponsored by the Office of Nuclear Regulatory Research, U.S. Nuclear Regulatory Commission, under FIN Numbers A22122 and A22562; Program Managers: Drs. J. Muscara and E. Woolridge.

References

1. *Criteria of Section III of the ASME Boiler and Pressure Vessel Code for Nuclear Vessels*, The American Society of Mechanical Engineers, United Engineering Center, New York, Library of Congress Catalog No. 56-3934 (1989).
2. J. B. Terrell, *Fatigue Life Characterization of Smooth and Notched Piping Steel Specimens in 288°C Air Environments*, NUREG/CR-5013, MEA-2232 (May 1988).
3. D. Weinstein, *BWR Environment Cracking Margins for Carbon Steel Piping-Final Report*, EPRI Report NP-2046, Electric Power Research Institute, Palo Alto, CA (1982).
4. D. Hale, S. A. Wilson, J. W. Kass, and E. Kiss, *Low Cycle Fatigue of Commercial Piping Steels in a BWR Primary Water Environment*, J. Eng. Mater. and Technol. **103**, 15-25 (1981).
5. K. Iida, H. Kobayashi, and M. Higuchi, *Predictive Method of Low Cycle Fatigue Life of Carbon and Low Alloy Steels in High Temperature Water Environments*, NUREG/CP-0067, MEA-2090, Vol. 2 (April 1986).
6. N. Nagata, S. Sato, and Y. Katada, *Low Cycle Fatigue Behavior of Low Alloy Steels in High Temperature Pressurized Water*, Structural Mechanics in Reactor Technol. **10**, 209-214 (1989-8).
7. J. B. Terrell, *Effect of Cyclic Frequency on the Fatigue Life of ASME SA-106-B Piping Steel in PWR Environments*, J. Mater. Eng. **10**, 193-203 (1988).
8. P. D. Hicks, in *Environmentally Assisted Cracking in Light Water Reactors: Semiannual Report October 1990—March 1991*, NUREG/CR-4667 Vol. 12, ANL-91/24, pp. 3-18 (August 1991).
9. T. A. Prater and L. F. Coffin, *The Use of Notched Compact-Type Specimens for Crack Initiation Design Rules in High-Temperature Water Environments*, Corrosion Fatigue: Mechanics Metallurgy, Electrochemistry, and Engineering, ASTM STP 801, T. W. Crooker and B. N. Leis, eds., American Society for Testing and Materials, Philadelphia, pp. 423-444 (1983).
10. T. A. Prater and L. F. Coffin, *Notch Fatigue Crack Initiation in High Temperature Water Environments: Experiments and Life Prediction*, J. of Pressure Vessel Technol., Trans. ASME, **109**, 124-134 (1987).
11 P. D. Hicks and F. P. A. Robinson, *Fatigue Crack Growth Rates in a Pressure Vessel Steel under Various Conditions of Loading and the Environment*, Met. Trans. **17A**, 1837-1849 (1986).
12. *Proc. of the Int. Atomic Energy Agency Specialists' Meeting on Subcritical Crack Growth*, NUREG/CP-0044, MEA-2014, Vols. 1 & 2 (May 1983).
13. *Proc. of the 2nd Int. Atomic Energy Agency Specialists' Meeting on Subcritical Crack Growth*, NUREG/CP-0067, MEA-2090, Vols. 1 & 2 (April 1986).
14. *Proc. of the 3rd Int. Atomic Energy Agency Specialists' Meeting on Subcritical Crack Growth*, NUREG/CP-0112, Vols. 1 & 2 (August 1990).

15. T. A. Prater, W. R. Catlin, and L. F. Coffin, *Surface Crack Growth Behavior of Structural Metals in High Temperature Water Environments*, J. Eng. Mater. Technol. **108**, 2–9 (1986).

16. M. O. Speidel and R. M. Magdowski, *Stress Corrosion Cracking of Nuclear Reactor Pressure Vessel Steel in Water: Crack Initiation versus Crack Growth*, Corrosion 88, Paper No. 283, St. Louis, MO (March 1988).

17. D. A. Hale, *The Effect of BWR Startup Environments on Crack Growth in Structural Alloys*, J. Eng. Mater. Technol. **108**, 44–49 (1986).

18. F. P. Ford and P. L. Andresen, *Stress Corrosion Cracking of Low-Alloy Pressure Vessel Steels in 288°C Water*, in Proc. 3rd Int. Atomic Energy Agency Specialists' Meeting on Subcritical Crack Growth, NUREG/CP-0112, Vol. 1, pp. 37–56 (August 1990).

19. P. M. Scott and D. R. Tice, *Stress Corrosion in Low-Alloy Steels*, Nucl. Eng. Des. **119**, 399–413 (1990).

20. J. Y. Park, in *Environmentally Assisted Cracking in Light Water Reactors: Semiannual Report April—September 1989*, NUREG/CR-4667 Vol. 9, ANL-90/48, pp. 10–17 (March 1991).

21. T. F. Kassner, W. J. Shack, W. E. Ruther, and J. Y. Park, in *Environmentally Assisted Cracking in Light Water Reactors: Semiannual Report April—September 1990*, NUREG/CR-4667 Vol. 11, ANL-91/9, pp. 3–8 (May 1991).

22. Proceedings of EPRI Workshop on Significance and Control of Chromate in BWRs, Chicago (November 13–14, 1990).

23. W. E. Ruther, W. K. Soppet, and T. F. Kassner, in *Environmentally Assisted Cracking in Light Water Reactors: Semiannual Report April—September 1988*, NUREG/CR-4667 Vol. 7, ANL-89/40, pp. 18–29 (March 1990).

24. W. E. Ruther, W. K. Soppet, and T. F. Kassner, in *Environmentally Assisted Cracking in Light Water Reactors: Annual Report October 1983—September 1984*, NUREG/CR-4287, ANL-85-33, pp. 93–101 (June 1985).

25. W. L. Clark and A. J. Jacobs, *Effect of Radiation Environment on SCC of Austenitic Materials*, in Proc. 1st Int. Symp. Environmental Degradation of Materials in Nuclear Power Systems – Water Reactors, National Association of Corrosion Engineers, Houston, pp. 451–461 (1984).

26. F. Garzarolli, D. Alter, and P. Dewes, *Deformability of Austenitic Stainless Steels and Ni-Base Alloys in the Core of a Boiling and Pressurized Water Reactor*, in Proc. 2nd Int. Symp. Environmental Degradation of Materials in Nuclear Power Systems – Water Reactors, National Association of Corrosion Engineers, Houston, pp. 131–138 (1986).

27. F. Garzarolli, D. Alter, P. Dewes, and J. L. Nelson, *Deformability of Austenitic Stainless Steels and Ni-Base Alloys in the Core of a Boiling and Pressurized Water Reactor*, in Proc. 3rd Int. Symp. Environmental Degradation of Materials in Nuclear Power Systems – Water Reactors, G. J. Theus and J. R. Weeks, eds., The Metallurgical Society, Warrendale, PA, pp. 657–664 (1988).

28. H. Hanninen and I. Aho-Mantila, *Environment-Sensitive Cracking of Reactor Internals*, ibid., pp. 77–92.

29. K. Fukuya, S. Nakahigashi, S. Ozaki, M. Teresawa, and S. Shima, *Grain Boundary Segregation of Impurity Atoms In Irradiated Austenitic Stainless Steels*, ibid., pp. 665–671.

30. A. J. Jacobs, G. P. Wozaldo, K. Nakata, T. Yoshida, and I. Masaoka, *Radiation Effects on the Stress Corrosion and Other Selected Properties of Type-304 and Type-316 Stainless Steels*, ibid., pp. 673–681.

31. E. P. Simonen and R. H. Jones, *Calculated Solute Segregation Kinetics Related to Irradiation Assisted Stress Corrosion Cracking*, ibid., pp. 683–690.

32. A. J. Jacobs, R. E. Clausing, L. Heatherly, and R. M. Kruger, *Irradiation-Assisted Stress Corrosion Cracking and Grain Boundary Segregation in Heat-Treated Type 304 SS*, in Effects of Radiation on Materials: 14th Int. Symp., Vol. I, ASTM STP 1046, N. H. Packan, R. E. Stoller, and A. S. Kumar, eds., American Society for Testing and Materials, Philadelphia, pp. 424–436 (1989).

33. A. J. Jacobs, R. E. Clausing, M. K. Miller, and C. Shepherd, *Influence of Grain Boundary Composition on the IASCC Susceptibility of Type 348 Stainless Steel*, in Proc. 4th Int. Symp. Environmental Degradation of Materials in Nuclear Power Systems – Water Reactors, National Association of Corrosion Engineers, Houston, pp. 14–21 to 14–45 (1990).

34. C. M. Shepherd and T. M. Williams, *Simulation of Microstructural Aspects of IASCC in Water Reactor Core Components*, ibid., pp. 14–11 to 14–20.

35. P. L. Andresen, F. P. Ford, S. M. Murphy, and J. M. Perks, *State of Knowledge of Radiation Effects on Environmental Cracking in Light Water Reactor Core Materials*, ibid., pp. 1–83 to 1–121.

36. S. Bruemmer, L. A. Charlot, and E. P. Simonen, *Grain Boundary Chemistry Effects on Irradiation-Assisted Stress Corrosion Cracking*, Corrosion 90, Paper No. 506, Las Vegas, NV (April 1990).

37. W. J. S. Yang, *Precipitation Evolution in Type 316 Stainless Steels Irradiated in EBR-II*, in Radiation-Induced Changes in Microstructure: 13th Int. Symp., ASTM STP 955, F. A. Garner, N. H. Packan, and A. S. Kumar, eds., American Society for Testing and Materials, Philadelphia, pp. 628–646 (1987).

38. A. Strasser, J. Santucci, K. Lindquist, W. Yario, G. Stern, L. Goldstein, and L. Joseph, *Evaluation of Stainless Steel Cladding in LWRs*, EPRI NP-2642, Electric Power Research Institute, Palo Alto, CA (December 1982).

39. H. M. Chung and W. E. Ruther, in *Environmentally Assisted Cracking in Light Water Reactors: Semiannual Report, October 1989–March 1990*, NUREG/CR-4667 Vol. 10, ANL-91/5, pp. 14–17 (March 1991).

40. H. M. Chung and W. E. Ruther, in *Environmentally Assisted Cracking in Light Water Reactors: Semiannual Report, April–September 1990*, NUREG/CR-4667 Vol. 11, ANL-91/9, pp. 16–22 (April 1991).

41. H. M. Chung and W. E. Ruther, in *Environmentally Assisted Cracking in Light Water Reactors: Semiannual Report, October 1990–March 1991*, NUREG/CR-4667 Vol. 12, ANL-91/24, pp. 37–54 (August 1991).

42. M. Kodama, S. Nishimura, J. Morisawa, S. Shima, S. Suzuki, and M. Yamamoto, *Effects of Fluence and Dissolved Oxygen on IASCC in Austenitic Stainless Steels*, 5th Int. Symp. Environmental Degradation of Materials in Nuclear Power Systems – Water Reactors, National Association of Corrosion Engineers (August 1991).

43. W. E. Ruther, W. K. Soppet, and T. F. Kassner, *Effect of Temperature and Ionic Impurities at Very Low Concentrations on Stress Corrosion Cracking of AISI 304 Stainless Steel*, Corrosion **44**, 791–799 (1988).

44. P. S. Maiya, *Prediction of Environmental and Strain-Rate Effects on the Stress Corrosion Cracking of Austenitic Stainless Steels*, J. Pres. Vessel Technol. **109**, 116–123 (1987).

45. P. S. Maiya, *Plastic Strain, Environmental, and Crevice Effects on SCC Initiation and Propagation in Types 316NG and 304 Stainless Steel*, Corrosion **45**, 915–924 (1989).

Distribution for NUREG/CR-4667, Vol. 13 (ANL-92/6)

Internal

W. J. Shack (30)

TIS File (3)

ANL Patent File

ANL Contract File

External

NRC, for distribution per R5

ANL Libraries (2)

Manager, Chicago Operations Office, DOE

Materials and Components Technology Division Review Committee:

- H. Berger, Industrial Quality Inc., Gaithersburg, MD
- M. S. Dresselhaus, Massachusetts Institute of Technology, Cambridge, MA
- S. J. Green, Electric Power Research Institute, Palo Alto, CA
- R. A. Greenkorn, Purdue University, West Lafayette, IN
- C.-Y. Li, Cornell University, Ithaca, NY
- P. G. Shewmon, Ohio State University, Columbus
- R. Smith, Electric Power Research Institute, NDE Ctr., Charlotte, NC

P. L. Andresen, General Electric Corporate Research and Development, Schenectady, NY

R. G. Ballinger, Massachusetts Institute of Technology, Cambridge, MA

W. H. Bamford, Structural Materials Engineering, Westinghouse Electric Corp., Pittsburgh

S. M. Bruemmer, Battelle Pacific Northwest Laboratory

J. A. Bonucci, Commonwealth Edison Co., Chicago

G. Cragnolino, Southwest Research Inst., San Antonio, TX

R. M. Crawford, Fluor-Daniel Corp., Chicago

D. Cubicciotti, Electric Power Research Inst., Palo Alto, CA

W. H. Cullen, Materials Engineering Assoc., Inc., Lanham, MD

R. Duncan, Combustion Engineering, Inc., Windsor, CT

M. Fox, APTECH, Tucson, AZ

Y. S. Garud, S. Levy, Inc., Campbell, CA

F. Garzarolli, KWU, Erlangen, Germany

B. M. Gordon, General Electric Co., San Jose, CA

H. E. Hanninen, Technical Research Centre of Finland, Finland

D. Harrison, USDOE, Germantown, MD

J. Hickling, MPA Stuttgart, Stuttgart, Germany

M. E. Indig, General Electric Co., Pleasanton, CA

H. S. Isaacs, Brookhaven National Laboratory

A. Jacobs, General Electric Co., San Jose, CA

L. James, Bettis Atomic Power Laboratory

R. H. Jones, Battelle Pacific Northwest Laboratory

T. Karlsen, OECD Halden Reactor Project, Halden, Norway

J. N. Kass, Lawrence Livermore National Laboratory

C. Kim, Westinghouse Electric Corp., Pittsburgh

L. Ljungberg, ASEA-ATOM, Vasteras, Sweden

C. D. Lundin, U. Tennessee, Knoxville, TN

D. D. Macdonald, Pennsylvania State University, University Park, PA

T. R. Mager, Westinghouse Electric Corp., Pittsburgh

H. Metha, General Electric Co., San Jose, CA

D. Morgan, Pennsylvania Power and Light Co., Allentown, PA

J. L. Nelson, Electric Power Research Inst., Palo Alto, CA

R. A. Oriani, U. Minnesota, Minneapolis

S. Ranganath, General Electric Co., San Jose, CA

E. J. Rowley, Commonwealth Edison Co., Chicago

P. M. Scott, Framatome, Paris, France

C. Shepherd, AEA Technology–Harwell Labs., Didcot, Oxon, UK

S. Smialowska, Ohio State U., Columbus

M. O. Speidel, Swiss Federal Institute of Technology, Zurich, Switzerland

D. M. Stevens, Lynchburg Research Center, Babcock & Wilcox Co., Lynchburg, VA

W. A. Van Der Sluys, Research & Development Division, Babcock & Wilcox Co., Alliance, OH

E. Venerus, Knolls Atomic Power Laboratory

J. R. Weeks, Brookhaven National Laboratory

D. Winkel, Teleco Oil Field Services, Meriden, CT

A. W. Zeuthen, Long Island Lighting Co., Wading River, NY

NUREG/CR–4667, Vol. 13

ENVIRONMENTALLY ASSISTED CRACKING IN LIGHT WATER REACTORS

MARCH 1992